Contents of issue 1 vol. LVII

Engineering Transactions, Vol. **LVII**, No. 1, pp. 1–68, Warszawa 2009

ENGINEERING TRANSACTIONS • *Engng. Trans.* • **57**, 1, 3–15, 2009
Polish Academy of Sciences • Institute of Fundamental Technological Research

DYNAMIC BUCKLING OF NON-SWAY IMPERFECT RECTANGULAR STEEL FRAMES

I. G. Raftoyiannis [1], A. N. Kounadis [2]

[1] **National Technical University of Athens**
Department of Civil Engineering
9 Iroon Polytechneiou St., Zografou Campus
Athens 15780, Greece

[2] **Academy of Athens**
Biomedical Research Foundation
4 Soranou Efessiou, Athens 11527, Greece

A nonlinear stability analysis is performed on non-sway rectangular two-bar steel frames subjected to a concentrated, suddenly applied joint load with constant magnitude and infinite duration. Using energy and geometric considerations, the dynamic buckling load is determined by considering the frame, being a continuous system, as a discrete 2 degrees-of-freedom system with corresponding coordinates of the two bar axial forces. The effect of imperfection sensitivity due to loading eccentricity is also addressed. A qualitative and quantitative analysis of these autonomous systems yields a substantial reduction of the computational work. The efficiency and reliability of the nonlinear stability analysis proposed herein is illustrated by several examples, which are also solved using finite element nonlinear analysis.

Key words: nonlinear dynamic stability, imperfect frames, suddenly applied load, loading eccentricity, FEM.

1. Introduction

In modern elastomechanics, *elastic stability theory* has attracted considerable attention due to the increasing demands in the design and analysis of light and stiff structures with high load-carrying capacity. A major contribution to this area is the initial post-buckling analysis of Koiter [1], which refers to systems that in their ideally perfect state exhibit a bifurcation point at the critical buckling load. However, the existence of ideally perfect structural systems is an exception rather than the rule. The majority of real structural systems, if accurately modeled, experiences limit point instability rather than bifurcational buckling. This is so because the presence of any small imperfection, which is unavoidable in actual systems, implies the degeneration of the bifurcation to a limit point [2].

The present work examines in detail the critical dynamic buckling response of non-sway, imperfect (due to loading eccentricity) two-bar frames, which are supported on two immovable hinges. It is qualitatively shown that this type of non-sway frames, associated from the onset of loading with (primary) bending, cannot exhibit any asymmetric bifurcation, losing always its stability via a limit point. However, the case of loss of stability via any asymmetric bifurcation can be considered only in an asymptotic sense. The first buckling load estimate, useful for the subsequent development, is readily obtained by employing a linear stability analysis. Thereafter, the nonlinear equilibrium equations of the latter frame are derived through a variational approach by employing the principle of stationary value of the total potential energy (TPE). These equations can be written in terms of the first derivatives of the TPE with respect to the unknown axial forces in the two bars. This is an important step, which facilitates the analysis, since we can consider the continuous system (i.e. the two-bar frame) as a two-degrees-of-freedom model, governed by two generalized coordinates, being the aforementioned axial forces in the two bars. Then, one can establish the second variation of the TPE as a function of the above mentioned two axial forces. By vanishing the stability determinant (i.e. the second variation of the TPE), written in terms of the second derivatives of the TPE, we obtain the condition governing the critical state [7, 12]. This condition, along with the equilibrium equations, leads to an easy and direct evaluation of the critical (buckling) load. Moreover, simultaneous vanishing of the TPE and the equilibrium equations lead to a lower bound estimate of the dynamic buckling load. This very simple procedure yields reliable results for structural design, proposed for the above type of dynamic loading associated with autonomous systems. Subsequently, more reliable results for the dynamic buckling load are obtained using the energy and geometric considerations of Kounadis approach recently presented in Ref. [16].

The methodology proposed herein is demonstrated by means of several numerical examples solved also by a nonlinear FEM, which subsequently are compared with those of previous analyses [8, 9].

2. Mathematical formulation

Consider the rectangular two-bar, geometrically perfect, frame ABC shown in Fig. 1 supported on two immovable hinges. Let ℓ_i, A_i and I_i be the length, cross-sectional area, and moment of inertia of the i-th bar ($i = 1, 2$). The frame is loaded at its joint B by a vertical concentrated force P, eccentrically applied with respect to the centerline of the vertical bar AB. The loading eccentricity e^* measured from the axis of the latter bar is positive if the point of application of the load is located to the right of this axis. The deformed configuration of the frame is described by the displacements w_i^* (transverse deflection) and ξ_i^* (axial displacement) at any point x_i^* of the centerline of the i-th bar. Both bars made of a Hookean material can undergo moderate rotations but small strains [4, 10, 11].

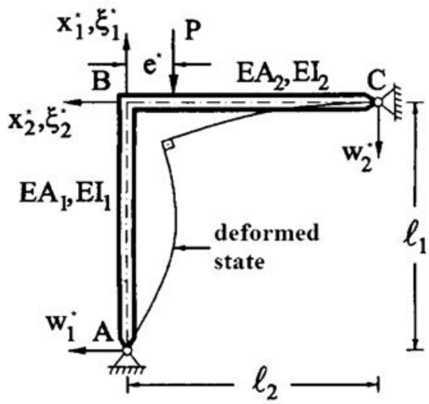

FIG. 1. Geometry and sign convention of an imperfect rectangular two-bar frame.

Introducing the dimensionless quantities

$$x_i = \frac{x_i^*}{\ell_i}, \quad w_i = \frac{w_i^*}{\ell_i}, \quad \xi_i = \frac{\xi_i^*}{\ell_i}, \quad k_i^2 = \frac{S_i \ell_i^2}{EI_i}, \quad \lambda_i^2 = \frac{A_i \ell_i^2}{I_i} \ (i = 1, 2), \tag{2.1}$$
$$e = \frac{e^*}{\ell_1}, \quad \beta^2 = \frac{P\ell_1^2}{EI_1}, \quad \rho = \frac{\ell_2}{\ell_1}, \quad \mu = \frac{I_2}{I_1},$$

the total potential energy (TPE) function V, in dimensionless form, is given by KOUNADIS [5]:

$$V = \frac{1}{2}\int_0^1 \left[\lambda_1^2 \left(\xi_1' + \frac{1}{2} w_1'^2\right)^2 + w_1''^2\right] dx_1 \tag{2.2}$$
$$+ \frac{\mu}{2\rho}\int_0^1 \left[\lambda_2^2 \left(\xi_2' + \frac{1}{2} w_2'^2\right)^2 + w_2''^2\right] dx_2 + \beta^2 \xi_1(1) + \beta^2 \rho e w_2'(1),$$

where the prime denotes differentiation with respect to x_i $(i = 1, 2)$. Note that the replacement of the eccentric joint load by a centrally applied load and a bending moment – related to the last term of Eq. (2.2) – presupposes that e is sufficiently small.

The geometric boundary conditions, known a priori, are given by

$$w_1(0) = w_2(0) = \xi_1(0) = \xi_2(0) = 0, \tag{2.3}$$
$$w'_1(1) = w_2'(1), \qquad \rho\xi_2(1) = w_1(1), \qquad \xi_1(1) = -\rho w_2(1).$$

Application of the principle of a stationary value of the TPE function, $\delta V = 0$, yields the following differential equations:

$$\left.\begin{aligned} \lambda_i^2\left(\xi_i' + \frac{1}{2}w_i'^2\right)' &= 0\\ w_i'''' - \left[\left(\xi_i' + \frac{1}{2}w_i'^2\right)w_i'\right]' &= 0 \end{aligned}\right\} i = 1, 2 \tag{2.4}$$

and natural boundary conditions after using Eqs. (2.3)

$$\begin{aligned} &w_1''(0) = w_2''(0) = 0,\\ &\lambda_1^2\left[\xi_1'(1) + \frac{1}{2}w_1'^2(1)\right] + \frac{\mu}{\rho^2}\left\{w_2'''(1) - \lambda_2^2\left[\xi_2'(1) + \frac{1}{2}w_2'^2(1)\right]w_2'(1)\right\} + \beta^2 = 0,\\ &\frac{\mu}{\rho^2}\lambda_2^2\left[\xi_2'(1) + \frac{1}{2}w_2'^2(1)\right] - w_1'''(1) + \lambda_1^2\left[\xi_1'(1) + \frac{1}{2}w_1'^2(1)\right]w_1'(1) = 0,\\ &w_1''(1) + \frac{\mu}{\rho}w_2''(1) + \rho\beta^2 e = 0. \end{aligned} \tag{2.5}$$

Integration of the first of Eqs. (2.4) gives

$$\xi_i'(x_i) + \frac{1}{2}w_1'^2(x_i) = -\frac{k_i^2}{\lambda_i^2} \qquad (i = 1, 2), \tag{2.6}$$

due to which the second of Eqs. (2.4) becomes

$$w_i''''(x_i) + k_i^2 w_i''(x_i) = 0 \qquad (i = 1, 2). \tag{2.7}$$

The general integrals of Eqs. (2.6) and (2.7) are

$$\begin{aligned} \xi_1(x_1) &= C - \frac{k_1^2}{\lambda_1^2}x_1 - \frac{1}{2}\int_0^{x_1} w_1'^2(x_1')dx_1',\\ \xi_2(x_2) &= \overline{C} - \frac{k_2^2}{\lambda_2^2}x_2 - \frac{1}{2}\int_0^{x_2} w_2'^2(x_2')dx_2',\\ w_1(x_1) &= C_1 \sin k_1x_1 + C_2 \cos k_1x_1 + C_3x_1 + C_4,\\ w_2(x_2) &= \overline{C}_1 \sin k_2x_2 + \overline{C}_2 \cos k_2x_2 + \overline{C}_3x_2 + \overline{C}_4, \end{aligned} \tag{2.8}$$

where the integration constants C, $\overline{C}$, C_i and $\overline{C}_i$ (for $i = 1, .., 4$) are determined by the boundary conditions.

Note that the unusual case of tension in the horizontal bar is not important. As shown by KOUNADIS *et al.* [8], this occurs for very small values of the external loading or in case of monotonically rising (stable) equilibrium paths.

Using Eqs. (2.6), the conditions (2.5), after taking into account that

$$w_1'''(x_1) + k_1^2 w_1'(x_1) = C_3 k_1^2$$

and

$$w_2'''(x_2) + k_2^2 w_2'(x_2) = \overline{C}_3 k_2^2,$$

are simplified as follows:

$$\begin{aligned} w_1''(0) = w_2''(0) &= 0, \\ k_2^2 \overline{C}_3 + \frac{\rho^2}{\mu}(\beta^2 - k_1^2) &= 0, \\ k_1^2 C_3 + \frac{\mu}{\rho^2} k_2^2 &= 0, \\ w_1''(1) + \frac{\mu}{\rho} w_2''(1) + \rho\beta^2 e &= 0. \end{aligned} \tag{2.9}$$

By virtue of the first four of geometric conditions (2.3) and the first two of conditions (2.8), we find $C = \overline{C} = C_2 = \overline{C}_2 = C_4 = \overline{C}_4 = 0$. Then, Eqs. (2.8) become

$$\begin{aligned} \xi_1(x_1) &= -\frac{k_1^2}{\lambda_1^2} x_1 - \frac{1}{2} \int_0^{x_1} w_1'^2(x_1') dx_1', \\ \xi_2(x_2) &= -\frac{k_2^2}{\lambda_2^2} x_2 - \frac{1}{2} \int_0^{x_2} w_2'^2(x_2') dx_2', \\ w_1(x_1) &= C_1 \sin k_1 x_1 + C_3 x_1, \\ w_2(x_2) &= \overline{C}_1 \sin k_2 x_2 + \overline{C}_3 x_2. \end{aligned} \tag{2.10}$$

Using the last two of Eqs. (2.10), the last one of the natural boundary conditions (2.9) and the fifth of geometric conditions (2.3), we obtain

$$\begin{aligned} C_1 k_1^2 \sin k_1 + \frac{\mu}{\rho} \overline{C}_1 k_2^2 \sin k_2 - \rho\beta^2 e &= 0, \\ C_1 k_1 \cos k_1 + C_3 - \overline{C}_1 k_2 \cos k_2 - \overline{C}_3 &= 0. \end{aligned} \tag{2.11}$$

The third and fourth of Eqs. (2.10) along with Eqs. (2.11) yield

$$C_1 = \frac{\rho\beta^2 e\cos k_2 + \frac{\mu}{\rho}\left[\frac{\rho^2}{\mu}\frac{\left(k_1^2-\beta^2\right)}{k_2^2} + \frac{\mu}{\rho^2}\frac{k_2^2}{k_1^2}\right]k_2\sin k_2}{k_1\left(k_1\sin k_1\cos k_2 + \frac{\mu}{\rho}k_2\cos k_1\sin k_2\right)},$$

$$\overline{C}_1 = \frac{\rho\beta^2 e\cos k_1 - \left[\frac{\rho^2}{\mu}\frac{\left(k_1^2-\beta^2\right)}{k_2^2} + \frac{\mu}{\rho^2}\frac{k_2^2}{k_1^2}\right]k_1\sin k_1}{k_2\left(k_1\sin k_1\cos k_2 + \frac{\mu}{\rho}k_2\cos k_1\sin k_2\right)}, \tag{2.12}$$

$$C_3 = -\frac{\mu}{\rho^2}\frac{k_2^2}{k_1^2}, \overline{C}_3 = \frac{\rho^2}{\mu}\frac{\left(k_1^2-\beta^2\right)}{k_2^2}.$$

The last two of geometric conditions (2.3) yield the nonlinear equilibrium equations, which due to Eqs. (2.10), become

$$C_1\sin k_1 + C_3 = \rho\left[-\frac{k_2^2}{\lambda_2^2} - \frac{1}{2}\int_0^1 w_2'^2 dx_2\right],$$

$$\rho(\overline{C}_1\sin k_2 + \overline{C}_3) = \frac{k_1^2}{\lambda_1^2} + \frac{1}{2}\int_0^1 w_1'^2 dx_1, \tag{2.13}$$

where

$$\int_0^1 w_1'^2 dx_1 = C_3^2 + 2C_1C_3\sin k_1 + \frac{C_1^2k_1^2}{2}\left(1+\frac{\sin 2k_1}{2k_1}\right),$$

$$\int_0^1 w_2'^2 dx_2 = \overline{C}_3^2 + 2\overline{C}_1\overline{C}_3\sin k_2 + \frac{\overline{C}_1^2k_2^2}{2}\left(1+\frac{\sin 2k_2}{2k_2}\right), \tag{2.14}$$

with C_i and $\overline{C}_i$ $(i = 1, 3)$ given in Eqs. (2.12).

By virtue of relations (2.12) and (2.14), Eqs. (2.13) yield two nonlinear equilibrium equations with respect to k_1^2 and k_2^2, which can be determined only numerically as functions of the external loading β^2 for given values of the parameters $\lambda_i (i = 1, 2)$, ρ, μ and e. The entire (prebuckling and postbuckling) equilibrium path, being of the implicit form:

$$\beta^2 = \beta^2(k_1, k_2; \lambda_1, \lambda_2, \rho, \mu, e), \tag{2.15}$$

is established only numerically by solving Eqs. (2.13) with respect to k_i $(i = 1, 2)$ for various levels of the load β^2 and given values of λ_1, λ_2, μ, ρ and e, and then by plotting it via the relationship β^2 versus k_i $(i = 1, 2)$ or, usually, β^2 versus $w_1(1)$, $w_1'(1)$, $\xi_1(1)$ or $\xi_2(1)$.

3. Static critical loads

Introducing into Eq. (2.2) the expressions given in Eqs. (2.10), after integration, we get the expression of the TPE function V in terms of the unknown axial forces k_1 and k_2, for given values of the parameters λ_i $(i = 1, 2)$, μ, ρ and e. The derivatives of V with respect to k_1 and k_2, denoted by V_1 and V_2, yield the two nonlinear equilibrium Eqs. (2.13), i.e.

$$\begin{aligned} V_1 &= C_1 \sin k_1 + C_3 + \rho \left[\frac{k_2^2}{\lambda_2^2} + \frac{1}{2} \int_0^1 w_2'^2 dx_2 \right] = 0, \\ V_2 &= \rho(\overline{C}_1 \sin k_1 + \overline{C}_3) - \left[\frac{k_1^2}{\lambda_1^2} + \frac{1}{2} \int_0^1 w_1'^2 dx_1 \right] = 0, \end{aligned} \tag{3.1}$$

where C_1, C_3, $\overline{C}_1$ and $\overline{C}_3$ are given by Eqs. (2.12), and the integrals by relations (2.14).

The critical state C (β_c, k_1^c, k_2^c) is obtained by the condition of vanishing of the determinant of the matrix $[V_{ij}]$ of the second variation $\delta^2 V^c$, evaluated at the critical state C, namely

$$\det[V_{ij}]^c = \left(V_{11}V_{22} - V_{12}^2\right)^c = 0, \tag{3.2}$$

where

$$V_{11} = \partial^2 V / \partial k_1^2,$$

$$V_{22} = \partial^2 V / \partial k_2^2,$$

$$V_{12} = V_{21} = \partial^2 V / \partial k_1 \partial k_2.$$

4. Dynamic critical loads

Such an autonomous system, if damping is ignored, is governed by the principle of conservation of total potential energy, TPE, Hamiltonian E between any two states, i.e.

$$E = K + V, \tag{4.1}$$

where K is the positive definite total kinetic energy and V is the TPE, respectively. For this undamped autonomous system under the above type of dynamic loading, the initial ($t = 0$) conditions imply zero displacements and velocities, which yield $K_{t=0} = V_{t=0} = 0$ and hence $E = 0$. Since throughout the motion $E = 0$, from Eq. (4.1) it follows that [3, 6, 14]

$$V = -K. \tag{4.2}$$

Namely, throughout the motion (including the instant of Dynamic Buckling) the TPE function V is negative (i.e. for $V > 0$ there is no motion, and thus no dynamic buckling). According to the Lagrange or Laplace dynamic global stability criterion [16], *dynamic buckling* (in the large) for autonomous systems is defined as that state for which an escaped motion becomes either unbounded or of a very large amplitude. The minimum load corresponding to this state is defined as dynamic buckling load (DBL).

For 1-DOF autonomous undamped systems, dynamic buckling occurs always through a *saddle* (equilibrium) point, and hence $K = 0$, which due to Eq. (4.2) yields $V = 0$. The exact DBL and the associated critical displacement are obtained by solving the system of Eqs. $V = V_1 = 0$.

For 2-DOF systems the DBL is obtained by the procedure presented in Ref. [16, 17]. A lower bound dynamic buckling load denoted by $\tilde{\beta}_D^2$ is obtained by the solution of Eq. (3.1) and $V = 0$.

5. Numerical results

Numerical results for various geometric configurations of frames are given in both the graphical and tabular forms. Figures 2 and 3 show the total potential energy $V = 0$ in the $w_1(1)$–$w_2(1)$ plane for various load levels β^2, for a rectangular frame with

$$\mu = \rho = 1,$$

$$\lambda_1 = \lambda_2 = 80$$

and loading eccentricity $e = 0.01$. Note that $V = 0$ represents a closed curve in the $w_1(1)$–$w_2(1)$ plane for load levels lower than $\beta^2 = 2.2149$ (Fig. 3a). For higher loads, $V = 0$ represents an open curve (Fig. 2b) in the aforementioned plane. The motion of the joint B is bounded for load levels lower than $\beta^2 = 2.4585$, becoming unbounded for higher loads. The solution technique for obtaining the V-curve is based on the Newton-Ralphson scheme, where the symbolic manipulator Mathematica 5.1 [13] has been employed. The joint motion is obtained by means of a FEM nonlinear solution.

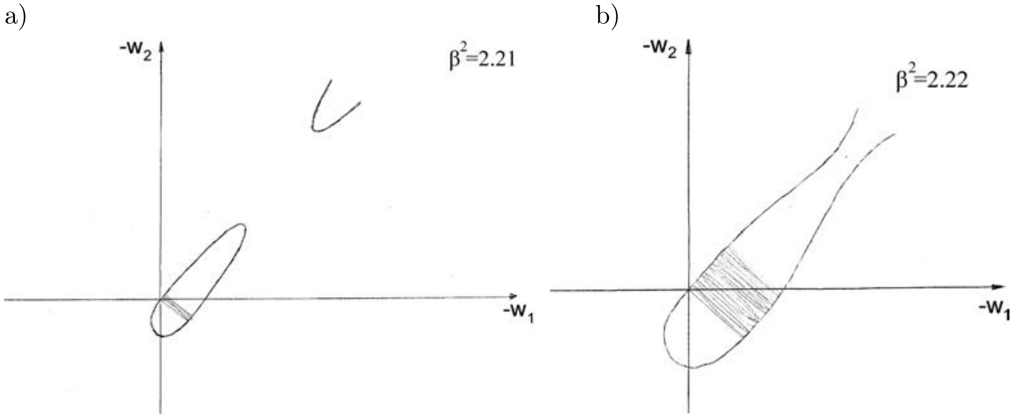

FIG. 2. Total potential energy V vs. $w_1(1)$–$w_2(1)$ for:
a) $\beta^2 = 2.21$ and b) $\beta^2 = 2.22$.

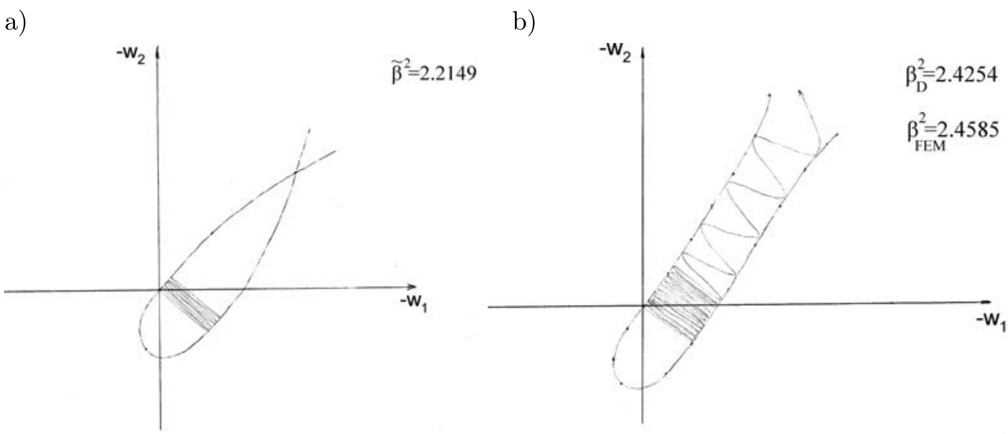

FIG. 3. Total potential energy V vs. $w_1(1)$–$w_2(1)$ for:
a) $\beta^2 = \tilde{\beta}^2 = 2.2149$ and b) $\beta_D^2 = 2.4254$.

In Table 1, one can see numerical values of the lower bound critical loads $\tilde{\beta}_D^2$ and the analytical and numerical dynamic buckling loads (DBL) β_D^2 with the corresponding values of loading eccentricities, slenderness ratios, moment of inertia and length ratios.

It is worth to mention that the maximum deviation in β^2 between the present analytical approach and the FEM results is less than 1.3%. However, the method proposed herein is less cumbersome and very efficient in parametric studies and can be more readily applied than a numerical FEM nonlinear analysis. The entire analysis is also facilitated by using qualitative considerations based on sufficient knowledge of the physical phenomenon of the problem under discussion.

Table 1. Critical DBL β^2 for loading eccentricity $e = 0.01$ and various values of μ, ρ, λ_1.

λ_1	μ	ρ	$\tilde{\beta}_D^2$	β_D^2
40	0.25	0.25	2.0189	2.2108 (2.2409)
		1	0.8909	0.9755 (0.9888)
		4	0.2626	0.2876 (0.2915)
	1	0.25	2.9596	3.2409 (3.2851)
		1	2.1745	2.3811 (2.4136)
		4	0.8949	0.9799 (0.9933)
	4	0.25	3.3251	3.6411 (3.6908)
		1	3.2985	3.6120(3.6613)
		4	2.1929	2.4013 (2.4340)
80	0.25	0.25	2.0564	2.2519 (2.2826)
		1	0.9074	0.9937 (1.0072)
		4	0.2675	0.2929 (0.2969)
	1	0.25	3.0146	3.3012 (3.3462)
		1	2.2149	2.4254 (2.4585)
		4	0.9115	0.9981 (1.0118)
	4	0.25	3.3869	3.7088 (3.7594)
		1	3.3598	3.6791 (3.7294)
		4	2.2336	2.4459 (2.4793)

Note: The values in parentheses correspond to results obtained by FEM.

A nonlinear finite element (FEM) analysis is also employed for obtaining the critical loads and studying the postbuckling behavior of the frame. For this purpose, the finite element package Algor is utilized [15]. With the aid of the "Superdraw" editor of Algor, the frame is modeled as a plane model in the XY-plane, where all out-of-plane displacements are restrained. Both the column and the beam are subdivided into 100 beam elements. Thus, the frame model has 602 degrees of freedom and 200 elements. Next, the boundary conditions (pinned supports) and the beam properties (material and sectional properties) are defined for all elements. A concentrated load P is dynamically applied at the joint B acting downwards, while the loading eccentricity is implemented in the form of a concentrated moment applied at the same joint of magnitude $M = -Pe$. In Fig. 4, the finite element model of a rectangular two-bar frame, created by Superdraw, is shown.

Next, with the aid of "Nonlinear Decoder" editor of Algor, where the solution technique and the loading parameters are set. Geometrical nonlinearity with large displacements is defined for the model, and the updated Lagrange method

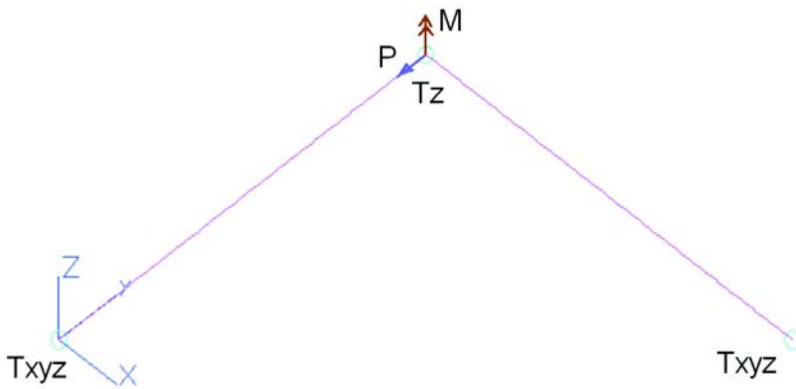

Fig. 4. Finite element model of a rectangular two-bar frame.

for solution of the nonlinear problem is chosen. Finally, the loading step size as well as the tolerance value is defined. Execution of the Nonlinear Decoder creates the input file for the nonlinear FE solver.

The nonlinear solver of the Algor package is used and the nonlinear solution is performed. The results are stored in the output file and can be viewed with the "Nonlinear Superview" editor of Algor. In Fig. 5, one can see the postbuckling deformation for the rectangular frame with eccentricity $e = 0.01$ obtained via the finite element method.

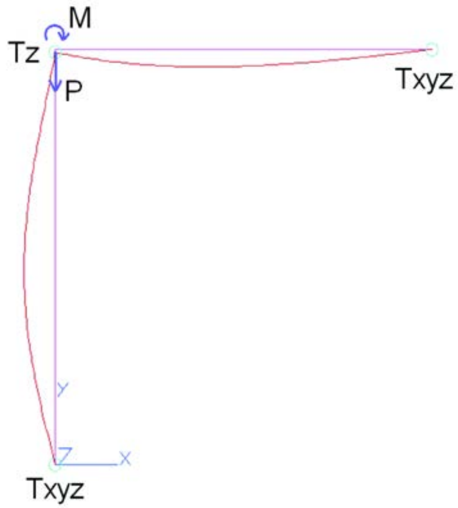

Fig. 5. Dynamic buckled shape of the rectangular frame with $e = 0.01$ obtained by FEM.

It is worth to notice that for the cases of frames with initial imperfections, there occurs inadequacy or unreliability of the results obtained via finite element analyses, which can be safely established by using the proposed technique which is essentially analytic. More specifically, using the conservation of energy principle for conservative systems, we see that after a large number of cycles (time-steps) the total potential energy V and the kinetic energy K do not cancel each other, as could be expected from the theoretical analysis. This justifies the slight deviation observed between the results obtained by FEM and the ones obtained analytically.

6. Concluding remarks

The most important conclusions of this study dealing with the nonlinear dynamic buckling response of a rectangular imperfect two-bar non-sway frame with various loading eccentricities, can be summarized as follows:

1. A systematic, comprehensive and readily applicable method for establishing the dynamic buckling loads of imperfect (due to loading eccentricity frames) is thoroughly discussed. This is facilitated by considering the total potential energy (TPE) as a function of the two axial bar forces. Thus, the continuous system (frame) is reduced to a 2 degrees-of-freedom system.
2. A qualitative discussion for seeking the dynamic buckling load based on geometrical considerations involving the TPE surface is properly established.
3. A direct and easily employed evaluation of the static critical buckling (limit point) load is established leading to very reliable results. To this end, the numerical part is appreciably reduced. Moreover, the analytical part can also be reduced if symbolic manipulation is employed.
4. The dynamic buckling loads for non-sway two-bar frames corresponding to a certain (non-zero) loading eccentricity are obtained for various geometrical parameters. The results are compared with the numerical ones obtained by a nonlinear FEM analysis.
5. The proposed approach proved to be very reliable and the computational effort is drastically reduced in case of multi-parameter analyses.

References

1. W. T. Koiter, *On the Stability of Elastic Equilibrium*, PhD Thesis presented to the Polytechnic Institute of Delft, The Netherlands 1945 (English translation NASA TT-F-10833, 1967).

2. J. M. T. Thompson and G. W. Hunt, *A general Theory of Elastic Stability*, John Wiley & Sons, London 1973.

3. G. I. Ioannidis, I. G. Raftoyiannis and A. N. Kounadis, *Nonlinear Buckling of Imperfect Systems with Symmetric Imperfections*, Archive of Applied Mechanics, **73**, 711–717, 2004.

4. D. O. Brush and B. O. Almroth, *Buckling of Bars, Plates, and Shells*, McGraw-Hill, New York, NY 1975.

5. A. N. Kounadis, *Dynamic Buckling of Simple Two-Bar Frames Using Catastrophe Theory*, Int. J. Non-Linear Mech., **37**, 1249–1259, 2002.

6. A. N. Kounadis, G. I. Ioannidis and X. Lignos, *Stability Analysis of a Two-Bar Frame Using Catastrophe Theory*, Proc. Eurosteel '02, Coimbra, Portugal, **1**, 149–61, 2002.

7. G. A. Simitses, *Elastic Stability of Structures*, Prentice Hall Inc., Englewood Cliffs, New Jersey 1976.

8. A. N. Kounadis, J. Giri and G. A. Simitses, *Nonlinear Stability Analysis of an Eccentrically Loaded Two-Bar Frame*, J. Appl. Mech., ASME, **44**, 4, 701–706, 1977.

9. G. A. Simitses and A. N. Kounadis, *Buckling of Imperfect Rigid-Jointed Frames*, J. Eng. Mech. Div., ASCE, **104**, EM3, 569–586, 1978.

10. A. N. Kounadis, *An Efficient Simplified Approach for the Nonlinear Buckling Analysis of Frames*, AIAA J., **23**, 8, 1254–1259, 1985.

11. A. N. Kounadis, *Efficiency and Accuracy of Linearized Postbuckling Analyses of Frames based on Elastica*, Int. J. Solids and Structures, **24**, 11, 1097–1112, 1988.

12. S. P. Timoshenko and J. M. Gere, *Theory of Elastic Stability*, McGraw-Hill, New York, NY 1961.

13. S. Wolfram, *Mathematica*, 4th ed., Version 4, Cambridge University Press, UK 1999.

14. G.I. Ioannidis and I. G. Raftoyiannis, *A Simplified Nonlinear Stability Analysis of an Imperfect Rectangular Two-Bar Frame*, Computational Mechanics, **35**, 2, pp. 127–133, 2004.

15. C. C. Spyrakos and I. G. Raftoyiannis, *Linear and nonlinear finite element analysis in engineering practice*, Algor Publ. Div., Pittsburgh, PA 1997.

16. A. N. Kounadis, *A Geometric Approach for Establishing Dynamic Buckling Loads of Autonomous Potential 2-DOF Systems*, J. Appl. Mech., ASME, **66**, 1, 55–61, 1999.

17. I. G. Raftoyiannis, G. T. Constantakopoulos, G. T. Michaltsos and A. N. Kounadis, *Dynamic Buckling of a Simple Geometrically Imperfect Frame using Catastrophe Theory*, Int. J. Mechanical Sciences, **48**, 1021–1030, 2006.

Received March 17, 2008; revised version November 24, 2008.

ENGINEERING TRANSACTIONS • *Engng. Trans.* • **57**, 1, 17–34, 2009
Polish Academy of Sciences • Institute of Fundamental Technological Research

PARAMETER SELECTION RULES FOR ELEMENTS OF ENERGY-ABSORBING STRUCTURES

S. Ochelski, T. Niezgoda

Military Academy of Technology
Department of Mechanics and Applied Computer Science
2 Kaliskiego Street, 00-908 Warsaw, Poland

The paper presents the results of an experimental program and gives suggestions on the design of an energy-absorbing structure with respect to the kinetic energy of impact. The presented results account for the influence of the following factors on the energy-absorbing capability: matrix and reinforcement type, structure, shape and thickness of elements.

Key words: polymer composites, absorption energy, experimental testing.

1. Introduction

On the basis of the literature review and the results of our own tests on energy absorbing structures it can be stated that, because of high strength-to-mass ratio, the polymer composites have a wide application in construction of energy-absorbing structures of vehicles and aircrafts. The magnitude of the absorbed

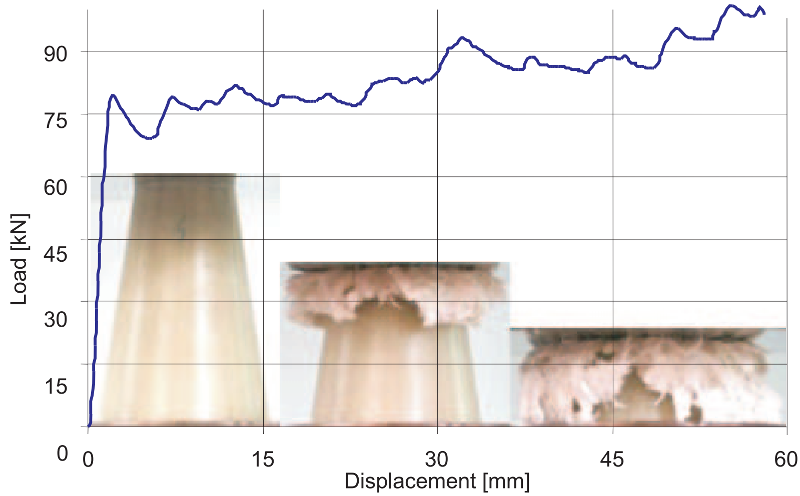

Fig. 1. $P - \Delta l$ dependence for a truncated cone-shaped specimen made of the epoxy composite reinforced with a glass mat.

energy depends both on the composite type and its components, from which the composite or the sandwich-type structure is made. The energy-absorbing structures, in particular those made of composites, with elements which can acquire various shapes, can be designed to reach the desired value of the absorbed energy, and the mechanism of progressive failure during crash will ensure obtaining of a high absorption energy.

In the paper, an extensive experimental program was carried out on the influence of the type and structure of composites, geometry and shape of an energy-absorbing element. Exemplary relations obtained from the tests were presented in Figs. 1 and 2, from which the progressive failure work has been determined.

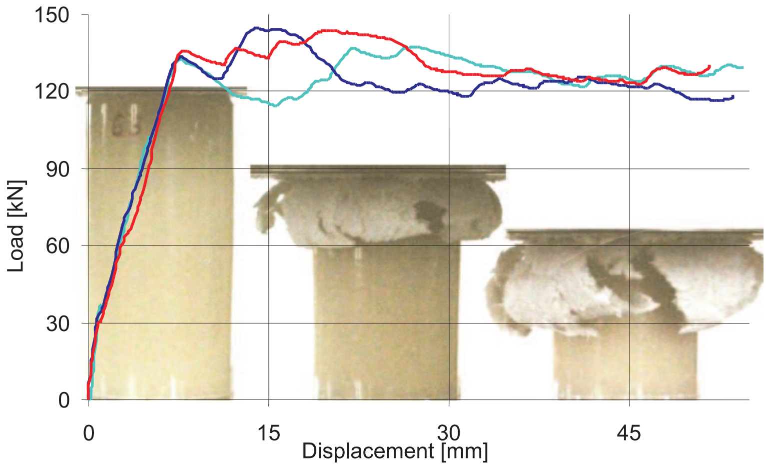

Fig. 2. Crush failure force dependence on displacement for 3 specimens made of the epoxy composite reinforced with a glass mat.

2. Selection of the energy-absorbing structure parameters depending on the crash energy value

It follows from the work – kinetic energy theorem that:

$$-\Delta E = L. \tag{2.1}$$

The negative increase in the kinetic energy ΔE resulting from the crash is equivalent to the work of the crush force L (absorbed energy)

$$-\Delta E = \frac{m \cdot V_k^2}{2} - \frac{mV_0^2}{2}, \tag{2.2}$$

where m is the object's mass, V_0 – initial velocity, V_k – final velocity.

Assuming the data obtained from an experimental test of a helicopter crash of a 767 kg mass and the impact velocity equal to 8 m/s, we have

$$\Delta E = \frac{767 \cdot 8^2}{2} = 24.544 \text{ kJ}, \tag{2.3}$$

which is equal to the absorbed energy (AE). Knowing the mass of the equipment and its impact velocity, one can calculate the energy value which the absorbing energy structure has to absorb during its failure. Assuming displacement $\Delta l =$ 0.1 m, simple calculations show that the mean crushing force P is:

$$P = \frac{\Delta E}{\Delta l} = 240 \text{ kN}. \tag{2.4}$$

Assuming that the energy-absorbing structure is of a sandwich type, one can use for its core elements in the shape of tubes, truncated cones, spheres and waved shells. The results of investigation for all these cases in the form of AE will be presented further in the paper.

3. Cost (price) of materials for the energy-absorbing structures

While selecting materials for energy-absorbing structures, the data included in Table 1 can be useful. To build the energy-absorbing structures of aircrafts, because of the required lightness, mainly various kinds of polymer composites with different types of reinforcement are used. The structure lightness is also important in the automobile industry, because a light car can reach higher accelerations at the same power of the engine. The polymer composites not only have the highest ratio of strength and stiffness to their density, but also the highest specific absorbed energy (SAE), in comparison to metals and their alloys.

The prices of one kilogram of materials given in Table 1 were taken from current price lists (for the year 2006), whereas the SAE values for metals were taken from our own investigations and from literature.

The results presented in Table 1 demonstrate that from among all polymer composites, the epoxy one reinforced with a glass mat reveals the most advantageous ratio of the SAE to the price, whereas it is the carbon steel which, because of its lowest price, proved to have the highest ratio from all the analysed composites and metals. The mean SEA values presented in Table 1 are obtained for various geometries of the absorbing energy structures for the given composite type.

Table 1. Comparison of SAE with the price of one kilogram for composites and metals.

Material	Price [USD/kg]	SAE [kJ]	SAE/Price
carbon/epoxy – composite reinforced with roving	60–135	82.3	1.37–0,61
carbon/epoxy – composite reinforced with fabrics	52-120	88.9	1.71–0.74
glass/epoxy – composite reinforced with roving	5.3–10.5	45.1	8.5–4.29
glass/epoxy – composite reinforced with fabrics	4.2–6.5	76.2	18.14–11.72
glass/epoxy – composite reinforced with a mat	2.4–3.2	67.9	28.2–21.21
carbon/PEEK	230–260	128.0	0.55–0.49
aramid/epoxy	60–120	60.1	1.0–0.5
glass/vinylester – composite reinforced with roving	5.1–9.8	50.9	9.98–5.1
glass/vinylester – composite reinforced with fabrics	4.0–5.9	86.1	21.5–14.5
vinylester composite reinforced with carbon roving	58.2–132.1	92.9	1.6–0.79
vinylester composite reinforced with carbon fabrics	53.8–116.7	99.1	1.8–0.85
aluminium alloy	1.4–1.7	18.1	12.9–10.6
carbon steel	0.4–0.9	27.8	69.5–30.8
stainless steel	2.7–3.2	26.8	9.9–8.4

4. Influence of matrix type (resin) and reinforcements (fibres) of polymer composites

In our investigation we used the matrices and fibres most commonly used in the energy-absorbing structures of aircrafts and automobiles. The following composites were subjected to tests: epoxy, vinylester and polyetherketone ones with carbon, glass and aramid reinforcements of various forms (continuous fibres, fabrics and mat). The results of investigation of the composite matrix influence on the SAE value are presented in Table 1.

On the grounds of the test results presented in Table 2 we can conclude that the highest value of the SAE is revealed by the composites with a polyetherketone matrix (PEEK), a slightly lower one – by those with a vinylester matrix, and a value considerably lower value than for the vinylester one – by the composites with an epoxy matrix.

The mechanical properties of composite's matrix influence considerably the crack resistance. The tests revealed that the more brittle is the composite matrix (low toughness), the lower becomes the crack resistance and, consequently, the absorbed energy AE.

Paper [1] presents the results of a critical investigation of energy release coefficients ($G_{i\mathrm{C}}$), with taking into account the influence of the matrix type and

Table 2. SAE comparison for various types of matrix of selected structures (G – glass fibres, C – carbon fibres, A – aramid fibres), under axial loading.

<table>
<tr><th colspan="2">Specimen shape</th><th>Structure</th><th>Epoxy composite SAE [kJ]</th><th>Vinylester composite SAE [kJ]</th><th>PEEK resin composite SAE [kJ]</th></tr>
<tr><td colspan="2" rowspan="12">Thin parallelepiped</td><td>Glass mat (G)</td><td>40.8</td><td>35.3</td><td>58.5</td></tr>
<tr><td>$[(0/90)_T]_8$ (G)</td><td>41.3</td><td>69.8</td><td>71.2</td></tr>
<tr><td>$[(\pm 45)_T]$ (G)</td><td>47.8</td><td>62.1</td><td>76.4</td></tr>
<tr><td>$[0]_9$ (S)</td><td>38.8</td><td>42.8</td><td>69.3</td></tr>
<tr><td>$[0/90_T/(\pm 45)_T/0]_S$ (G)</td><td>36.8</td><td>51.7</td><td>62.1</td></tr>
<tr><td>$[(0/90)_8$ (C)</td><td>67.7</td><td>70.3</td><td>92.5</td></tr>
<tr><td>$[(\pm 45)_T]$ (C)</td><td>65.1</td><td>68.9</td><td>89.3</td></tr>
<tr><td>$[0]_9$ (C)</td><td>62.4</td><td>64.9</td><td>86.9</td></tr>
<tr><td>$[0/90_T/(\pm 45)_T/0]_S$ (C)</td><td>60.8</td><td>62.9</td><td>81.8</td></tr>
<tr><td>$[(0/90)_8$ (A)</td><td>48.1</td><td>59.2</td><td>62.8</td></tr>
<tr><td>$[(\pm 45)_T]$ (A)</td><td>47.9</td><td>60.7</td><td>65.2</td></tr>
<tr><td>$[0/90_T/(\pm 45)_T/0]_S$ (A)</td><td>47.4</td><td>58.3</td><td>63.4</td></tr>
<tr><td colspan="2" rowspan="10">Tubes</td><td>$[0_3]$ (G)</td><td>41.9</td><td>42.8</td><td>76.2</td></tr>
<tr><td>$[\pm 15/0_2]_S$(G)</td><td>47.5</td><td>49.3</td><td>80.3</td></tr>
<tr><td>$[\pm 30/0_2\ ]_S$ (G)</td><td>32.6</td><td>36.6</td><td>79.8</td></tr>
<tr><td>$[\pm 45/0_2]_S$ (G)</td><td>53.4</td><td>57.9</td><td>86.4</td></tr>
<tr><td>$[90/0_2]_S$ (G)</td><td>48.6</td><td>68.9</td><td>82.5</td></tr>
<tr><td>$[(0/90)_T/0_2]_S$ (G)</td><td>64.2</td><td>72.9</td><td>87.1</td></tr>
<tr><td>$[\pm 15/0_2]_S$(C)</td><td>71.3</td><td>73.3</td><td>94.9</td></tr>
<tr><td>$[\pm 30/0_2\ ]_S$ (C)</td><td>62.1</td><td>64.7</td><td>84.8</td></tr>
<tr><td>$[90/0_2]_S$ (C)</td><td>75.1</td><td>76.1</td><td>96.1</td></tr>
<tr><td>$[(0/90)_T/0_2]_S$ (C)</td><td>77.2</td><td>80.2</td><td>98.2</td></tr>
<tr><td rowspan="16">Truncated cone $\phi=$</td><td>5°</td><td rowspan="4">$(0/90)_T/0/(0/90)_T$ (G)</td><td>61.1</td><td>63.1</td><td>–</td></tr>
<tr><td>10°</td><td>59.6</td><td>62.5</td><td>–</td></tr>
<tr><td>15°</td><td>48.9</td><td>52.7</td><td>–</td></tr>
<tr><td>20°</td><td>35.8</td><td>38.9</td><td>–</td></tr>
<tr><td>5°</td><td rowspan="4">$[(0/90)_T]_2/0_2/[(0/90)_T]_2$ (G)</td><td>70.2</td><td>74.2</td><td>–</td></tr>
<tr><td>10°</td><td>69.8</td><td>71.3</td><td>–</td></tr>
<tr><td>15°</td><td>67.8</td><td>69.9</td><td>–</td></tr>
<tr><td>20°</td><td>61.6</td><td>64.2</td><td>–</td></tr>
<tr><td>5°</td><td rowspan="4">$(0/90)_T/0/(0/90)_T$ (C)</td><td>69.9</td><td>72.3</td><td>–</td></tr>
<tr><td>10°</td><td>67.3</td><td>70.6</td><td>–</td></tr>
<tr><td>15°</td><td>55.8</td><td>60.2</td><td>–</td></tr>
<tr><td>20°</td><td>43.1</td><td>52.9</td><td>–</td></tr>
<tr><td>5°</td><td rowspan="4">$[(0/90)_T]_2/0_2/[(0/90)_T]_2$ (C)</td><td>77.3</td><td>80.2</td><td>–</td></tr>
<tr><td>10°</td><td>76.8</td><td>78.5</td><td>–</td></tr>
<tr><td>15°</td><td>75.4</td><td>75.9</td><td>–</td></tr>
<tr><td>20°</td><td>68.9</td><td>71.8</td><td>–</td></tr>
</table>

Table 3. SAE comparison for various types of epoxy composite reinforcements for selected structures.

Specimen shape		Structure	Carbon roving	Carbon fabric	Glass roving	Glass fabric	aramid fabric
Plane		$[0_8]$	62.4	–	40.2	–	–
		$[(\pm 45)_T]$	-	65.1	-	47.8	47.9
		$[(0/90)_T]_{10}$	-	67.7	-	41.3	48.1
		$[0/90_T/(\pm 45)_T/0]_S$	–	60.8	–	36.8	47.4
Tubes		$[0_8]$	62.4	–	41.9	–	–
		$[\pm 15/0_2]_S$	71.3	–	47.5	–	–
		$[\pm 30/0_2\ ]_S$	62.1	–	32.6	–	–
		$[\pm 45/0_2]_S$	56.8	–	53.4	–	–
		$[90/0_2]_S$	75.1	–	48.6	–	–
		$[(0/90)_T/0_2]_S$	–	87.4	–	64.2	57.5
Truncated cone $\phi=$	5°	$(0/90)_T/0/(0/90)_T$	–	73.4	–	70.2	–
	10°		–	76.8	–	69.8	–
	15°		–	75.4	–	67.8	–
	20°		–	68.9	–	61.6	–
	5°	$[(0/90)_T]_2/0_2/[(0/90)_T]_2$	–	69.9	–	61.1	–
	10°		–	67.3	–	59.6	–
	15°		–	55.8	–	48.9	–
	20°		–	43.1	–	35.8	–

the load application manner (I, II, (I+II)) on the crack propagation effect (delamination) for static loads. Two types of composites were taken in the tests: an epoxy composite reinforced with unidirectional carbon fibres and one with a thermoplastic shield (PEEK) reinforced in the same way. The results of crack toughness tests for the investigated composites are presented in Table 4, where G_{IC} denotes the critical energy release coefficient. In tests, for different load cases (I, II, (I+II)) – (I – crack divergence, II – transversal shear, I+II – mixed load), the specimens DCB, ENF, CLS were assumed correspondingly – cf. paper [2].

Table 4. Matrix type influence on $\mathbf{G_{IC}}$ for the carbon fibre-reinforced composites.

Composite type	G_{IC} [J/m^2]	$G_{\mathrm{(I\text{-}II)C}}$ [J/m^2]	G_{IIC} [J/m^2]
Composite C/E	473	599	650
Composite C/PEEK	1205	1397	1502

From among all the analysed composites, the one with a thermoplastic matrix PEEK, reinforced with carbon fibres, proved to be the most resistant to cracking.

It can be concluded from the results presented in Table 3 that the carbon fibres composites reveal the highest impact energy-absorbing capability, whereas the aramid fibres-reinforced ones exhibit the lowest ability. This phenomenon can be explained by the mechanical properties of the fibres. The carbon fibres have high compression and shear strength and during failure the composites undergo shear and bending of the layers. However, the aramid fibres have a very low compression strength (R^{-}) but a very high tensile one ($R^{+} = 1300$ MPa), which is shown in Fig. 3.

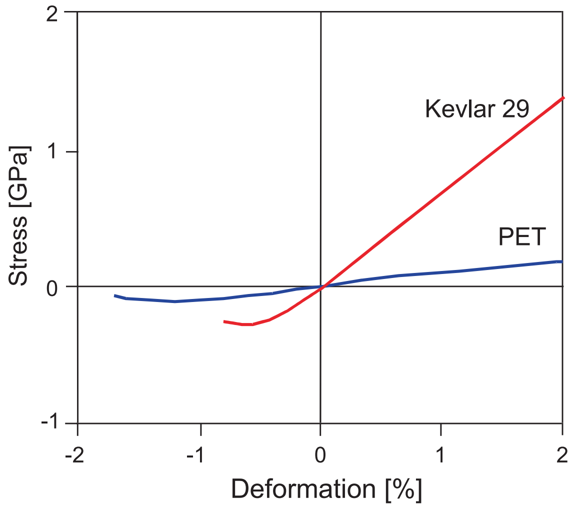

Fig. 3. The ε–σ diagram for Kewlar 29 and polyethylene terephthalate fibres [3].

The behaviour of the epoxy composite reinforced with aramid fibres in an axial compression test was dominated by the brittle matrix and plastic fibres, which resulted in a fast progress of delamination, with plastic deformations of the fibres' layer during the failure. The mechanical properties and, in particular, the bending stiffness of the layer with aramid fibres, are lower than those for the layers reinforced with carbon and glass fibres – the AE in the case of the aramid composite was lower.

5. Influence of the composite's structure

On the grounds of our own investigation, the influence of the composite's structure on the SAE was elaborated. The obtained results are shown in Figs. 4–8.

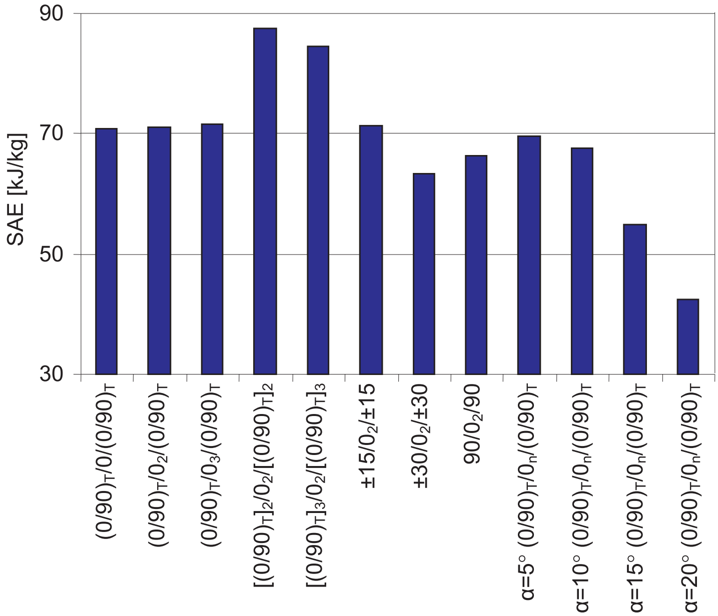

Fig. 4. Dependence of the energy-absorbing capability on the carbon-epoxy composite structure.

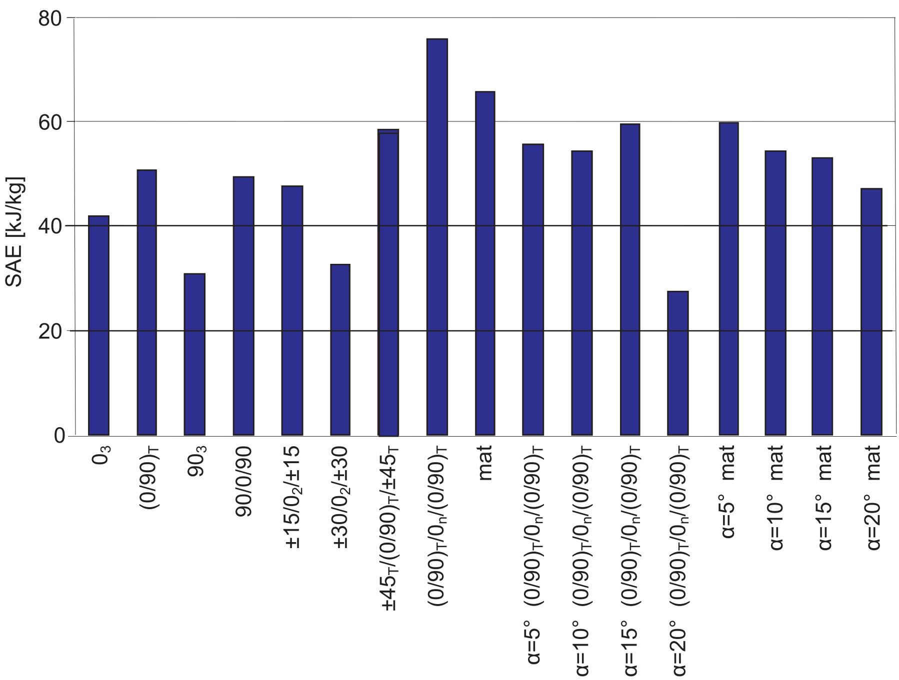

Fig. 5. Dependence of the energy-absorbing capability on the glass-epoxy composite structure.

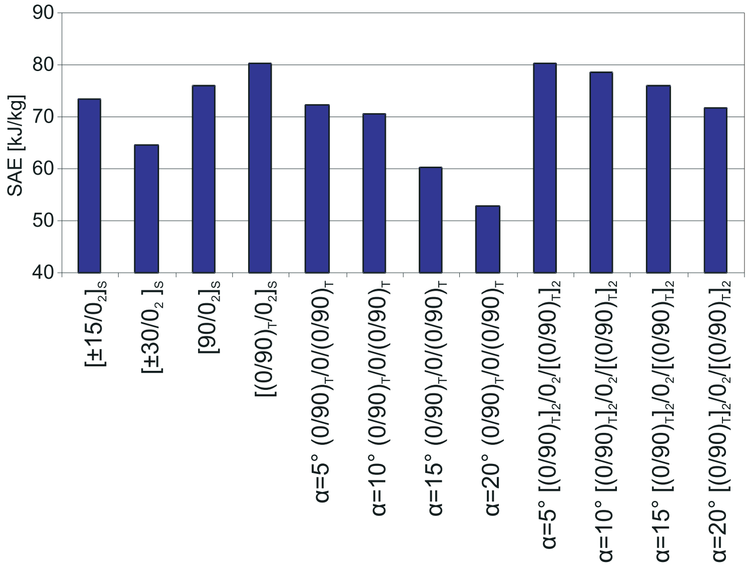

Fig. 6. Dependence of the energy-absorbing capability on the carbon-vinylester composite structure.

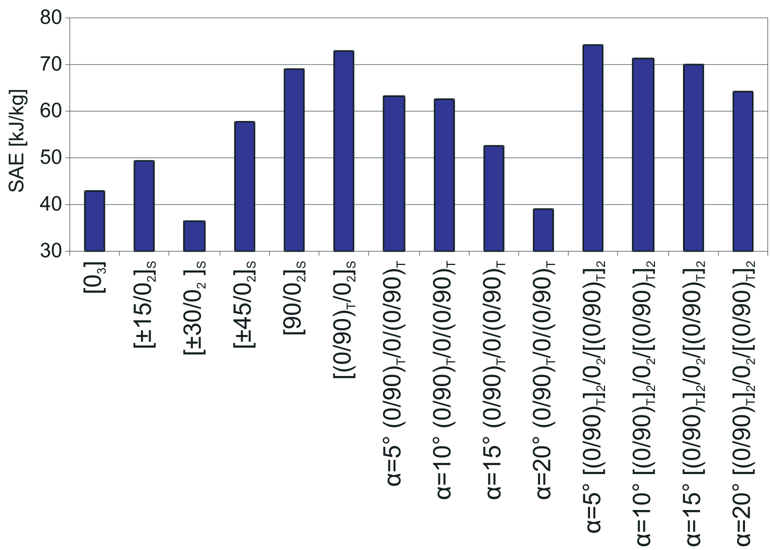

Fig. 7. Dependence of the energy-absorbing capability on the glass-vinylester composite structure.

The fibre orientation in a layer exerts the same influence on the SAE as on the mechanical properties, i.e. bending stiffness, failure deformations at tension and compression as well as on strength. The influence of the fibre orientation in a layer on the properties of the investigated composite and the composite

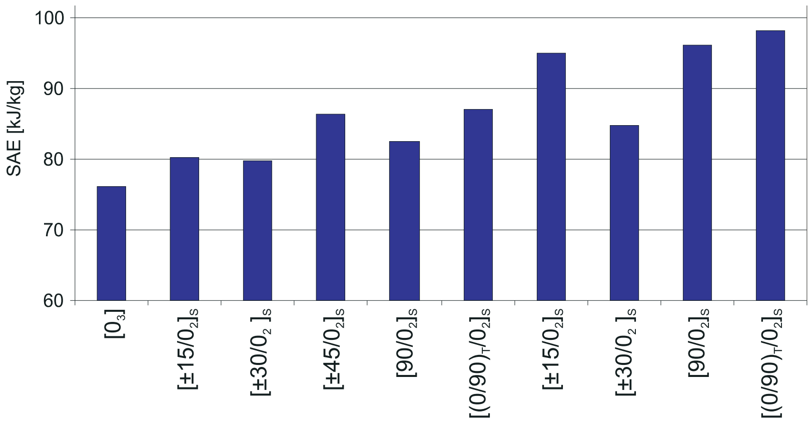

Fig. 8. Dependence of the energy-absorbing capability on the glass-PEEK composite structure.

response to the bending load during the test is clearly demonstrated in the case of a specimen reinforced with carbon fibres. The test results for the C/E $[+45_k/-45_k]_s$ composite revealed a higher crush failure force than for the composites of the structure $[0]_n$ and $[90]_n$, in spite of their lower stiffness. The C/E specimens with the $[+45_k/-45_k]_s$ structure exhibit a larger plastic range in the test, which makes an important difference in comparison to the crush process of other C/E specimens.

The highest SAE is exhibited by the elements of the $[(0/90)_T/0_n/(0/90)_T]$ structure, made of a carbon fibre-reinforced composite, in which the external and internal layers are made of cross-linked rowing fibres, which carry on the circumferential stresses, whereas the external layers consist of rowing parallel to the specimen's axis, which causes an increased compressive and bending strength.

6. Influence of the wall thickness of energy-absorbing structure elements

The basis for elaborating the SAE dependence on the element wall's thickness were the results of our own test, presented in Fig. 9, in which these relations are to a great extent approximated by straight lines. Very thin elements fail by local buckling, which is caused by low value of the SAE. The relation SAE-thickness of an energy-absorbing element can serve in practice to design an energy-absorption structure of a vehicle or an aircraft with a requested value of AE.

With a given kinetic energy of the crash, one can calculate the required absorption energy and next, while selecting the sandwich structure, assume the appropriate wall thickness of an element used as a core in the shape of a tube, a truncated cone, a sphere or a waved shell.

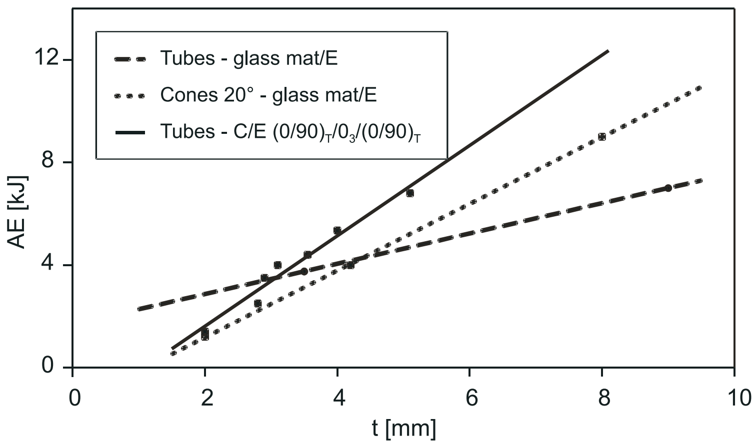

FIG. 9. Dependence of AE on the element wall's thickness.

The dependence of the AE on the element's thickness is very significant and clearly visible in the energy absorption tests. The composite's thickness influences the bending stiffness and failure of composite elements, which is clearly visible from the slope of the force-displacement curve in the first stage. A larger thickness results in a larger moment of inertia and a larger bending stiffness (EI), which in turn causes an increase of the bending resistance of the element and in the force necessary to reach the required failure deformation. Along with the increase of thickness, the composite layers become more stiff and they require higher deformation and failure forces.

The bending stiffness (EI), and in particular the specimen's thickness, affects the composite's AE, because the moment of inertia of the cross-section depends on the third power of the stiffness ($\mathrm{I} = wt^3/12$). The bending stiffness depends, of course, on the Young's modulus E, which in turn depends on the type and structure of the composite.

7. Influence of the layer's thickness in the composite on the SAE

In order to study the influence of the layers' thickness in the composite on the SAE value, the results of tests shown in Tables 5 and 6 were used. The dependence of the SAE on the ratio of the middle layer wall thickness t_m of the composite in respect to the external one (t_m/t_e), for carbon-epoxy and glass-epoxy composites is given in Fig. 11. From this relation it follows that for the glass-epoxy composite the maximum value of SAE occurs at $t_m/t_e \approx 3.0$. However, in the case of the carbon-epoxy composite the SAE is independent of the layer ratio (t_m/t_e).

Table 5. Properties of specimens made of carbon-epoxy composite.

Specimen number	Structure	α [°]	t [mm]	D_i [mm]	t_i [mm]	t_m [mm]	t_e [mm]	h [mm]	z [%]	m [g]	$P_{\max}$ [kN]	P_{avg} [kN]	AE [J]	SAE [kJ/kg]
1–4	$(0/90)_T/0/(0/90)_T$	5	1.2	59.5	0.4	0.4	0.4	75.0	42	22.8	24.4	21.4	1602	70.3
2–4	$(0/90)_T/0_2/(0/90)_T$	5	2.0	59.4	0.5	1.0	0.5	85.6	42	39.5	39.5	32.3	2761	69.9
3–4	$(0/90)_T/0_3/(0/90)_T$	5	2.2	59.5	0.4	1.4	0.4	83.4	42	42.2	46.2	34.7	2896	68.6
6–4	$(0/90)_T/0/(0/90)_T$	10	1.2	59.4	0.4	0.4	0.4	78.8	42	21.5	21.5	17.0	1336	62.2
7–4	$(0/90)_T/0_2/(0/90)_T$	10	2.4	59.7	0.6	1.2	0.6	83.6	42	41.3	44.8	35.1	2924	70.8
8–4	$(0/90)_T/0_3/(0/90)_T$	10	3.2	59.8	0.6	2.0	0.6	84.9	42	71.0	72.8	58.4	4924	69.4
11–4	$(0/90)_T/0/(0/90)_T$	15	1.2	58.8	0.4	0.4	0.4	54.1	42	17.4	18.1	16.5	892	51.3
12–4	$(0/90)_T/0_2/(0/90)_T$	15	2.0	59.2	0.5	1.0	0.5	58.0	42	23.7	27.3	22.8	1322	55.8
13–4	$(0/90)_T/0_3/(0/90)_T$	15	3.2	58.9	0.6	2.0	0.6	62.4	42	42.0	52.5	38.9	2426	57.8
16–4	$(0/90)_T/0/(0/90)_T$	20	1.2	79.5	0.4	0.4	0.4	67.0	42	25.2	14.7	13.6	911	36.4
17–4	$(0/90)_T/0_2/(0/90)_T$	20	2.0	78.8	0.5	1.0	0.5	68.9	42	36.0	27.9	22.5	1552	43.1
18–4	$(0/90)_T/0_3/(0/90)_T$	20	2.5	79.5	0.5	1.5	0.5	68.4	42	49.9	40.0	34.7	2373	47.6
21–4	$(0/90)_T/0/(0/90)_T$	0	1.7	39.3	0.6	0.5	0.6	98.2	42	28.5	21.1	27.7	2075	70.9
24–4	$(0/90)_T/0_2/(0/90)_T$	0	2.3	39.3	0.6	1.1	0.6	98.0	42	35.6	25.4	32.2	2489	71.0
28–4	$(0/90)_T/0_3/(0/90)_T$	0	3.0	39.3	0.6	1.8	0.6	102.2	42	54.6	39.4	54.5	4027	71.6
2–5	$[(0/90)_T]_2/0_2/[(0/90)_T]_2$	0	3.0	39.3	1.0	1.0	1.0	80.2	41	41.6	65.1	49.0	2586	87.4
5–5	$[(0/90)_T]_2/0_2/[(0/90)_T]_2$	5	2.1	59.5	0.7	0.7	0.7	76.3	41	35.7	43.9	35.67	2722	76.2
6–5	$[(0/90)_T]_2/0_2/[(0/90)_T]_2$	10	2.1	59.8	0.7	0.7	0.7	77.3	41	36.4	45.8	37.25	2879	79.1
7–5	$[(0/90)_T]_2/0_2/[(0/90)_T]_2$	15	2.1	59.3	0.7	0.7	0.7	50.6	41	24	64.2	36.16	1830	76.2
8–5	$[(0/90)_T]_2/0_2/[(0/90)_T]_2$	20	2.4	79.4	0.8	0.8	0.8	66.1	41	50.4	68.3	48.58	3211	63.7
9–5	$[(0/90)_T]_3/0_2/[(0/90)_T]_3$	0	3.6	39.3	1.4	0.8	1.4	81.2	42	50.1	67.5	52.34	4250	84.5
11–5	$[(0/90)_T]_3/0_2/[(0/90)_T]_3$	5	2.9	59.2	1.1	0.7	1.1	83.5	42	49.4	57.8	45.92	3834	77.6
12–5	$[(0/90)_T]_3/0_2/[(0/90)_T]_3$	10	2.9	60.1	1.1	0.7	1.1	82.8	42	53.5	57.7	49.43	4093	76.5
13–5	$[(0/90)_T]_3/0_2/[(0/90)_T]_3$	15	3.2	59.3	1.2	0.8	1.2	58.7	42	44.5	72.1	56.41	3311	74.4
14–5	$[(0/90)_T]_3/0_2/[(0/90)_T]_3$	20	4.2	79.5	1.6	1.0	1.6	68.4	42	81.3	116	83.34	5700	70.1
16–5	$\pm15/0_2/\pm15$	0	4.1	39.3	1.4	1.3	1.4	80.5	57	67.9	73.1	60.16	4843	71.3
18–5	$\pm30/0_2/\pm30$	0	3.8	39.3	1.3	1.2	1.3	81.2	59	56.1	58	42.92	3485	62.1
21–5	$90_2/0_2/90_2$	0	4.1	39.3	1.4	1.3	1.4	81.2	56	63.5	67	52.63	4274	67.3

Table 6. Properties of specimens made of glass-epoxy composite.

Specimen number	Structure	α [°]	t [mm]	D_i [mm]	t_i [mm]	t_m [mm]	t_e [mm]	h [mm]	z [%]	m [g]	$P_{\max}$ [kN]	P_{avg} [kN]	AE [J]	SAE [kJ/kg]
1–1	mat	0	3.5	39.3	–	–	–	86.7	35	59.4	52.6	43.8	3788	63.7
4–1	mat	0	9	39.3	–	–	–	91	35	168.3	137.4	117.7	10706	63.6
7–1	mat	5	2	60	–	–	–	91.2	35	35.9	20.7	16.6	1511	42.1
8–1	mat	5	2.7	61.6	–	–	–	93.2	35	65.7	47	39.2	3646	55.5
9–1	mat	5	4	61	–	–	–	91.1	35	100.1	70.2	59.5	5415	54.2
10–1	mat	5	5.2	59.6	–	–	–	92	35	123.4	88.4	75.6	6955	56.4
11–1	mat	10	1.5	61	–	–	–	82.3	35	31.7	18.9	15.6	1279	40.4
12–1	mat	10	1.8	62.4	–	–	–	85.2	35	36.5	26.1	20.2	1717	47.0
13–1	mat	10	2.3	60.4	–	–	–	86.3	35	46	34.3	24.9	2141	46.6
14–1	mat	10	3.2	60.6	–	–	–	91.9	35	68.4	54.7	42.1	3831	56.0
15–1	mat	10	4.2	60.6	–	–	–	91.7	35	81.4	72.6	56	5096	62.6
16–1	mat	10	5.5	61	–	–	–	84.3	35	111.4	99.7	80.8	6787	60.9
18–1	mat	15	3.4	59.2	–	–	–	62.6	35	48.4	56.9	41.8	2592	53.5
19–1	mat	15	4.2	59.6	–	–	–	62.3	35	59.9	69.1	54.7	3391	56.6
20–1	mat	15	5	60	–	–	–	62.5	35	73.9	88.3	67.6	4191	56.7
21–1	mat	15	6.4	60.2	–	–	–	62.4	35	99.2	132.3	98.5	6107	61.6
22–1	mat	20	2	80	–	–	–	70.8	35	45.5	27.5	18.6	1302	28.6
23–1	mat	20	4.2	80.6	–	–	–	70.2	35	92.4	77.5	59.2	4144	44.8
24–1	mat	20	8	79	–	–	–	64.2	35	162.3	175.5	143.5	9184	56.6
1–2	$90/0_2/90$	0	2.4	39.3	0.6	1.2	0.6	80.9	55	37.5	21.9	18.6	1597	42.6
4–2	$(\pm 45_T)_2/0_2/(\pm 45_T)_2$	0	3.4	39.3	1.1	1.2	1.1	90.1	49	53.4	34.1	31.7	2853	53.4
7–2	$[\pm 45_T]_2$	0	1.4	39.3	–	–	–	59.9	45	20.0	13.8	11.0	659	32.9
11–2	$[(0/90)_T]_2$	0	1.4	39.3	–	–	–	60.1	46	19.9	15.9	13.2	791	40.1
1–3	$90/0/90$	0	2	39.3	0.7	0.6	0.7	96	58	43.4	34.5	20.3	1953	45.0
4–3	$90_2/0_2/90_2$	0	3.7	39.3	1.2	1.3	1.2	89.8	56	84.8	62.5	51.0	4582	54.0
7–3	$90_3/0_3/90_3$	0	5.2	39.3	1.7	1.8	1.7	94.4	56	128.3	75.6	66.3	6260	48.8
10–3	$[(0/90)_T]_2/0_2/[(0/90)_T]_2$	0	4.5	39.3	1.5	1.5	1.5	94.7	49	79.8	66.8	62.7	5921	74.1
13–3	$[(0/90)_T]_4/0_4/[(0/90)_T]_4$	0	7	39.3	2.3	2.4	2.3	97.3	48	150.7	164.2	120.0	11680	77.4
16–3	$(\pm 45_T)_2/[(0/90)_T]_2/(\pm 45_T)_2$	0	4.5	39.3	1.5	1.5	1.5	92.6	44	84.1	69.0	53.0	4895	58.4
19–3	$\pm 15/0_2/\pm 15$	0	4.5	39.3	1.5	1.5	1.5	99.1	55	97.3	50.2	41.0	4070	47.5
22–3	0_3	0	2.5	39.3	–	–	–	96.6	54	50.7	32.1	22.0	2126	41.9
25–3	90_3	0	3	39.3	–	–	–	80.7	55	60.3	32.8	23.0	1856	30.8
27–3	$\pm 30/0_2/\pm 30$	0	4.4	39.3	1.5	1.4	1.5	93.6	56	94.7	43.3	33.0	3085	32.6

The obtained different relations for glass-epoxy and carbon-epoxy composites result from the difference in adhesion of fibres to the epoxy resin, which in the case of carbon fibres is larger than for the glass fibres. Moreover, the shear resistance in the planes parallel to the fibres, for composites of the $[0°]_{\mathrm{n}}$ structure, for the carbon-epoxy composite is 20.6 MPa and for the glass epoxy one – only 8.8 MPa, which means that for the carbon-epoxy composites it is 2.3 times higher. For $t_m/t_e = \infty$, i.e. for the carbon-epoxy composite of the $[0°]_{\mathrm{n}}$ structure, the SAE value is 76.2 kJ, which is approximately equal to the averaged SAE value for $t_m/t_e = (1-5)$.

The results of testing, averaged from several tests and included in Tables 5 and 6, are determined by characteristic quantities, denoting as follows (see Fig. 10):

$P_{\max}$ – maximum crush failure force, i.e. the first peak on the $P - \Delta l$ curve, which demonstrates the failure initiation;
AE – absorbed energy, equivalent to the area under the $P - \Delta l$ curve;
P_{avg} – average crush failure force ($P_{\mathrm{avg}} = \mathrm{AE}/\Delta l_{\max}$);
SAE – specific absorbed energy SAE $= \mathrm{AE}/m_c$, where m_c is the mass of the destroyed part of the specimen;
α – cone vertex half-angle;
t – wall thickness;
D_i – internal diameter (for a cone – the major diameter or the base diameter);
t_i – thickness of the internal layer;
t_m – thickness of the middle layer;
t_e – thickness of the external layer;
h – height of the specimen;
z – weight content of fibres in the composite;
m – mass of the specimen;
γ – force uniformity index ($P_{\mathrm{avg}}/P_{\max}$).

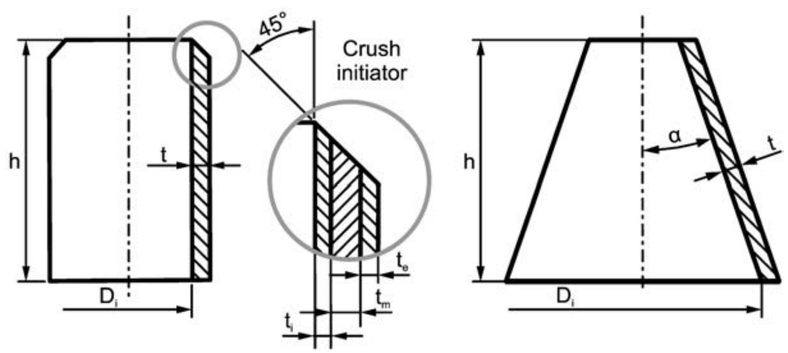

FIG. 10. Shapes of specimens used in tests.

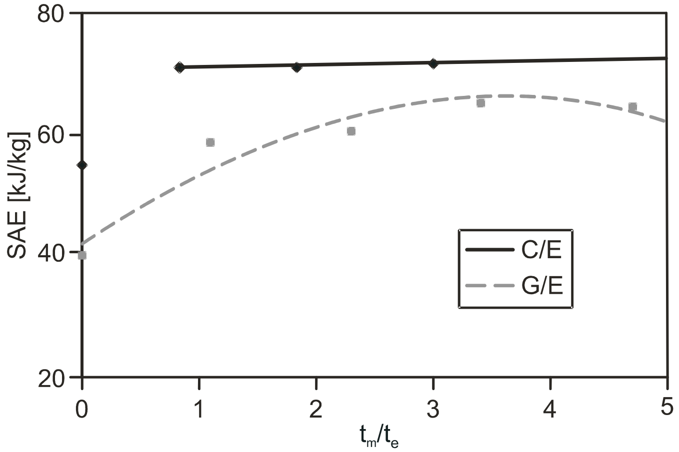

Fig. 11. Influence of the composite layers' thickness on the SAE.

8. Influence of the energy-absorbing structures' elements on the SAE (for selected structures)

It follows from the data presented in Table 7 that the highest SAE value is exhibited by the energy absorbing elements in the shape of a tube with a ring cross-section; next come truncated cones, plane shells and waved shells; the lowest SAE is revealed by spheres. The lowest value of SAE for the element in the shape of a sphere is caused by its specific failure mode. During failure, neither brittle fragmentation of the element's wall occurs nor the fibres' cracking takes place. Instead, the sphere's wall is bent into inside with permanent deformation, which is presented in Fig. 12.

Fig. 12. Cross-section of the destroyed sphere shows delamination of the plays.

It should be underlined that the influence of the shape of an energy-absorbing structure element is important not only from the point of view of the SAE value, but also because of the dependence of the acceleration during impact. In order

Table 7. Comparison of SAE for different shapes of the energy-absorbing elements.

Composite type	Structure	Plane element	Tube	Truncated cone	Waved shell	Spherical shell
G/E	mat	40.8	63.5	55.3 (5°) 44.8 (20°)	38.9	11.8
G/E	$[(0/90)_T]_S$	41.3	44.2	51.1 (5°) 35.8 (20°)	39.5	24.3
G/E	$[(\pm 45)_T]_n$	47.8	53.4	56.5 (5°) 38.3 (20°)	30	
G/E	$[(0/90)_T/0_2]_S$	44.1	64.2	61.2 (5°) 36.8 (20°)		
C/E	$[0]_n$	62.4	72.8	–	–	–
C/E	$[\pm 15/0_2]_S$	62.0	71.3	–	–	–
C/E	$[\pm 30/0_2]_S$	58.0	62.1	–	–	–
C/E	$[\pm 45/0_2]_S$	65.1	58.4	–	–	–
C/E	$[(0/90)_T/0]_S$	67.7	75.1	69.9 (5°) 43.1 (20°)	72.1	–
A/E	$[\pm 45/0_2]_S$	62.0	57.9	–		–
A/E	$[(0/90)_T/0]_S$	52.6	68.9	–	–	13.6
G/VE	$[0]_n$	42.8	42.8	–	–	–
G/VE	$[(\pm 45)_T]$	52.1	57.9	–	–	–
G/VE	$[(0/90)_T/0]_S$	49.8	72.9	63.1 (5°) 38.9 (20°)	–	–
C/VE	$[0]_n$	69.6	64.9	–	–	–
C/VE	$[(0/90)_T]_n$	70.7	75.7	–	–	–
C/VE	$[\pm 45]_n$	56.8	64.7	–	–	–
G/PEEK	mat	58.5	76.2	–	–	–
G/PEEK	$[(0/90)_T]_n$	71.2	82.5			

to determine the influence of the specimen's shape on the acceleration course at impact, we shall analyse the $P - \Delta l$ dependence obtained from tests for tubes, truncated cones, waved shells and spheres – Fig. 13.

On the grounds of the above results for the $P - \Delta l$ dependence, for specimens of the same thickness we conclude that the largest change of the crush failure force during loading and – consequently – a large SAE is exhibited by the energy-absorbing elements in the shape of tubes and corrugated shells, whereas a lower SAE was revealed by truncated cones and the lowest one – by spheres. Analogically to the load change, the maximum peaks of acceleration will occur during impact.

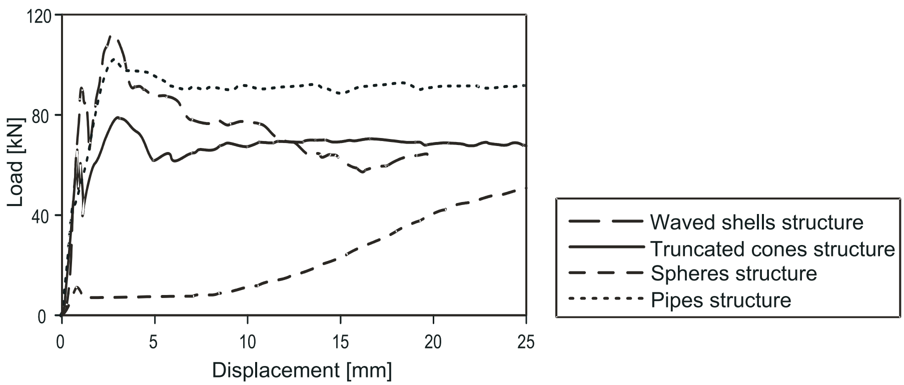

FIG. 13. $P - \Delta l$ dependence for a tube, a truncated cone, a waved shell and a sphere made of epoxy composite reinforced with a glass mat.

9. Summary

1. Exhaustive results of investigation presented in this paper and preliminary calculations included in its first part enable us to design an energy-absorbing structure with a programmed value of absorption energy of a given equipment under axial loading.
2. From all the analysed materials for energy-absorbing structures, the polymer composites are the most expensive, which was shown in Table 1, but a relatively cheap epoxy composite reinforced with a glass mat revealed in testing a relatively high AE with respect to its density.
3. The influence of the matrix type (resin) in a composite on the SAE is considerable. A large part in the ability of energy absorption is due to the mechanical properties of the matrices, in particular – their crack resistance. Brittle matrices, such as epoxy ones, reveal a lower ability of energy absorption, whereas the composites with a polyetherketone matrix proved to have the highest SAE.
4. The influence of the reinforcement type on the SAE is the following: carbon fibres have the highest SAE, whereas the aramid ones – the lowest. The carbon fibres have highest compressive and shearing strength, whereas for the aramid ones both strengths are low.
5. On the basis of various structures testing, one can conclude that the energy-absorbing structure should contain stiff and resistant middle layers, whereas the external ones should carry well the transversal stresses (circumferential in the case of a pipe). The influence of fibres orientation in an energy-absorbing element is the same on the bending and shear strength. The highest SAE was obtained for the $[(0/90)_T/0_n/(0/90)_T]$ structure with

the external layers made of fabric and the internal one – of continuous fibres aligned parallel to the compressive force.

6. The influence of the wall thickness of an energy-absorbing element on the SAE was presented in Fig. 7. Along with the increase of wall's thickness, the SAE increases because the bending strength of the wall grows also and it is the layers' bending that prevails in the failure process. Also, the influence of the layers' thickness in the composite on the SAE was considered. It was found that the ratio of the middle layer thickness to that of the external layers for the carbon fibre-reinforced composite is small.

References

1. S. Mall, K. T. Yun, N. K. Kochhar, *Characterization of matrix toughness effect on cyclic delamination growth in graphite fiber composites*, Composite Materials, Fatigue and Fracture, **2**, 1989.
2. S. Ochelski, *Experimental methods in the mechanics of structural composites* [in Polish], WNT, Warsaw 2004.
3. S. Kawabata, Y. Yamashita, M. Niwa, *Micro-mechanics of wool single fibre*, 10th International Wool Textile Research Conference, Aachen, Germany 2000.

Received June 2, 2008; revised version October 22, 2008.

ENGINEERING TRANSACTIONS • *Engng. Trans.* • **57**, 1, 35–43, 2009
Polish Academy of Sciences • Institute of Fundamental Technological Research

ANALYSIS OF ELASTIC PROPERTIES OF THIN-WALLED STRUCTURES DESIGNED BY SADSF METHOD

I. Markiewicz

Kielce University of Technology
Al. Tysiąclecia Państwa Polskiego 7, 25-314 Kielce, Poland

The paper presents the results of analyses of elastic properties of thin-walled structures designed by means of the SADSF method, carried out in order to confirm its practical usefulness. The SADSF method makes it possible – without applying any iterative correction procedures – to effectively solve the problems of design of such structures. The method can be applied in cases when only boundary conditions are given. The obtained solutions are free of the structural errors which can significantly deteriorate load carrying ability of structures of this class.

Key words: design, thin-walled structures, limit analysis, FEM analyses.

1. Introduction

The results of analyses presented in this paper are a part of an extensive program aimed at investigating actual properties of thin-walled constructions, whose structure, e.g. the number of component elements, their spatial allocation and the system of mutual connections, as well as the initial shape and dimensions of the elements, are determined by using the method of statically admissible discontinuous stress fields, SADSF [1, 9, 11].

In this paper, the author concentrates on three examples of structures, which were designed by W. Bodaszewski with application of its own, original software [1, 2]. These are:

- bent box section with corners (Fig. 1a);
- constructional joint created in the area of connection between two bent sections, of box and double-tee types, whose axes coincide in one straight line (Fig. 1b);
- constructional joint created in the area of connection between a box section subjected to torsion, and a twin-tee section subjected to bending (Fig. 1c).

The FEM analyses must be carried out because the SADSF method does not concern the elastic range, which is usually the range of exploitation load of the structure. One considers only the limit state of the structure, which pertains to

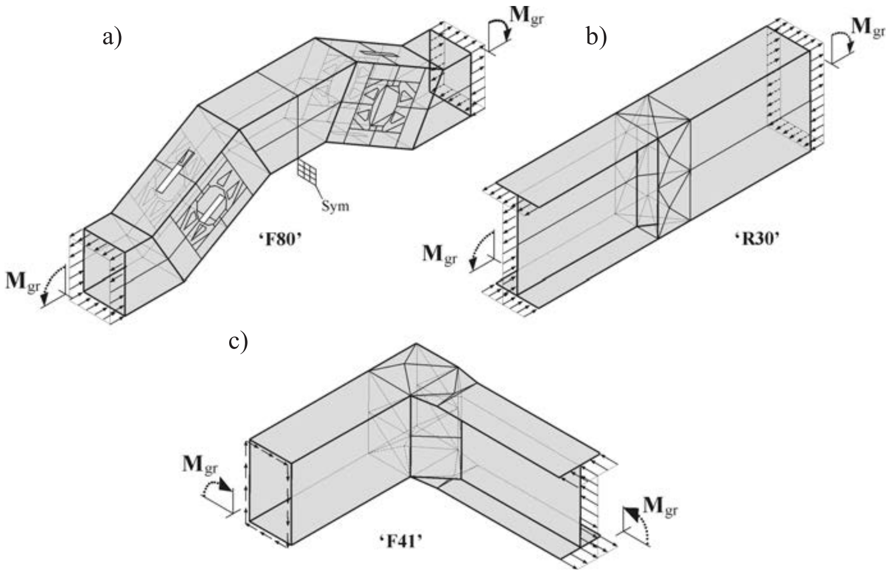

FIG. 1. Contours of statically-admissible stress fields determining shapes and dimensions of models of structures analyzed in this work ([1,2]).

the beginning of its collapse. It is also assumed that the collapse arises in the form of plastic flow, in which plane state of stress still exists in each component element. In the method, one uses a rigid-plastic model of the material, and the statically admissible stress fields which satisfy only equilibrium conditions and do not exceed the assumed yield condition at any point.

Despite these limiting assumptions, the structures designed by the SADSF method have several positive properties, which have been confirmed by numerical and experimental investigations. It has been confirmed, among other things, that membrane states of stress dominate in the elastic range, stress concentration is low, and material effort is well equalized in the whole volume of the structure – or at least along its free boundaries [1, 3, 4, 7, 8]. Such properties are difficult to obtain by traditional methods, which are based on designer's experience and intuition. On the other hand, one must be particularly careful when applying advanced methods based on consecutive iterative corrections to this class of structures. Generally speaking, de Saint Venant's principle does not apply to these cases, so that even small changes of constructional details may result in radical changes of load-carrying ability [1, 2, 8].

The fundamental advantage of systems designed by the SADSF method is that their structures are correctly selected to match the assumed loads. It means that it is possible to transmit the whole assumed load only through membrane forces. The errors made when selecting the structure can not be eliminated by changing dimensions of its elements. FEM analyses can only confirm inferior quality of the preliminarily designed structure, but they can not hint at any direction of possible improvement [1, 8].

The SADSF method can be applied already at the very beginning of the design process, when only boundary conditions are known [1, 2]. The task of the designer is reduced to selecting ready-made particular solutions from the library of the application version of the method's software [1, 2, 5, 12] and connecting them – like the Lego blocks – to form the structure. At the same time, one must keep the assumed boundary conditions and the conditions of equilibrium at the joined edges.

2. Calculational models

The analyses were carried out by means of the finite element method (FEM) using the system CosmosM. In the analyses, one assumes:

- linearly-elastic physical model of material and small strains;
- triangular shell elements of 3 nodes and 6 degrees of freedom in a node type SHELL3;
- average size of finite elements equal to 2–3 thicknesses of the element;
- loads equal to a half of the limit load value assumed in the design; distributions of loads consistent with the beam formulae used in the mechanics of materials for elastic range.

Additionally, one assumes:

- yield point of $\sigma_{\mathrm{pl}} = 300$ MPa for determining the limit load value; it means that, if one could obtain an ideal level of effort, the intensity of equivalent stress would be $\sigma_{\mathrm{eq}} = 150$ MPa at each point of the analysed structure;
- shape and dimensions of the analysed models nearly the same as those of the contours obtained from the solutions to design problems; small corrections of external contours introduced only in the vicinity of corners by rounding them with arches drawn outside of external boundaries. Within the inner contours, the inscribed circular holes are tangent to their boundaries (the problem of boundary corrections was not undertaken).

The analyses carried out in this work have an approximate character. Due to the fact that one operates on a shell model, local three-dimensional states in the vicinity of common borders between component elements are not analysed.

3. General results of analyses

In order to facilitate reviewing the obtained results, we first formulate a list of results which, because of their repeatability, seem to lead to general conclusions. Then, in all of the analysed cases one can find:

1. Domination of membrane states; the values of effort related to the bending state are small.
2. Relatively low concentrations of stress, and similar levels of maximal effort in all component elements.
3. Almost ideally-equalised fields of effort in torsion sections (Fig. 1c). In sections subjected to bending, well-equalised state of effort was found only in flanges, because of the existence of harmful states in these sections, characteristic for the bending axis.

The results obtained for all structure models are illustrated in the same way by the graphs. First, one presents the shape of analysed model with the assumed boundary conditions, then the distributions of equivalent stresses, in the Huber-Mises sense, to the component states of membrane and bending type.

4. Detailed results

4.1. Bent box-type section with corners

Because the structure is symmetrical, and so is the field of internal forces in it, we analysed only a half of the structure (Fig. 2a). On the symmetry plane β-β, we assumed appropriate boundary conditions, additionally introducing displacements that prevented the possibility of rigid motion. The load of bending moment was applied in the cross-section α-α consistently with the beam-type distribution used in mechanics of materials.

The distributions of stresses obtained for the component states, of membrane and bending type, are shown in Figs. 2b–d. By inspection of these distributions, one can see:

- In the membrane state (Figs. 2b,c):
  - formation of harmful states associated with the axis of elastic bending;
  - relatively good equalisation of effort in large areas of the flanges, and very similar levels of effort at the places of maximal effort;
  - low stress concentrations (maximal equivalent stress 215.5 Pa is not much greater than that which would exist when uniform effort was obtained in the whole volume of the structure, i.e. 150 MPa).
- In the bending state (Fig. 2d):
  - well-equalised effort field of very low value, which only locally reaches 7.75% of effort values associated with membrane state (16.7/215.5) – the maximal equivalent stress of 106.1 MPa appearing in the corner of the loaded boundary is not taken into account, because it results from the assumed boundary conditions.

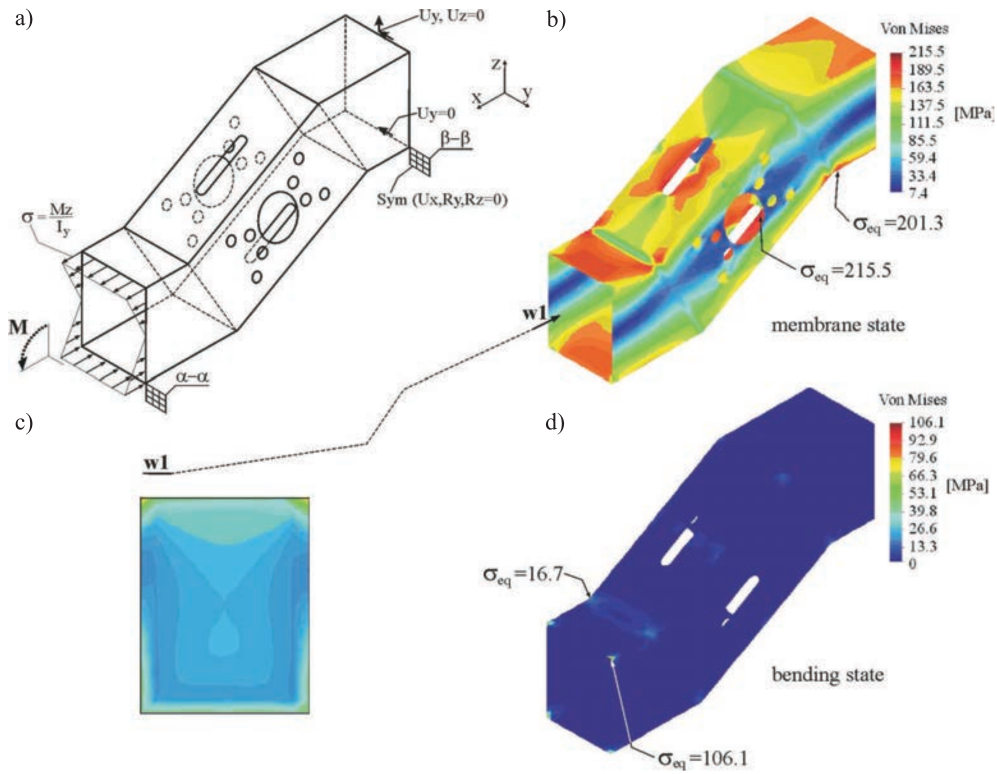

Fig. 2. Shape of a symmetric half of the analysed structure along with the assumed boundary conditions and obtained distributions of equivalent stresses.

Using the SADSF method, we obtain both the structure of the system, and shapes and dimensions of its component elements. What would happen, if one changed the structure designed by the SADSF method by removing one of its elements? Let this element be the diaphragm, for which an additional view of membrane stress distribution is shown in Fig. 2c. Inserting it into the structure (welding it in) is difficult; on the other hand, stresses in the diaphragm seem to be relatively low.

Distributions of equivalent stresses obtained for such a case are shown in Fig. 3. As it can be seen, the mentioned change in the structure caused almost a threefold increase of local equivalent stresses in membrane state (628/215.5), and over fifteenfold increase of it in bending state (260.2/16.7).

Despite the fact that such a dramatic increase of maximal stress concentrations was obtained, the changed structure still has the ability of transmitting the assumed load in membrane state (the structure remains a proper one). If such a possibility would not exist, the deterioration of load-carrying ability would have been even worse, and would affect the whole structure [1, 8].

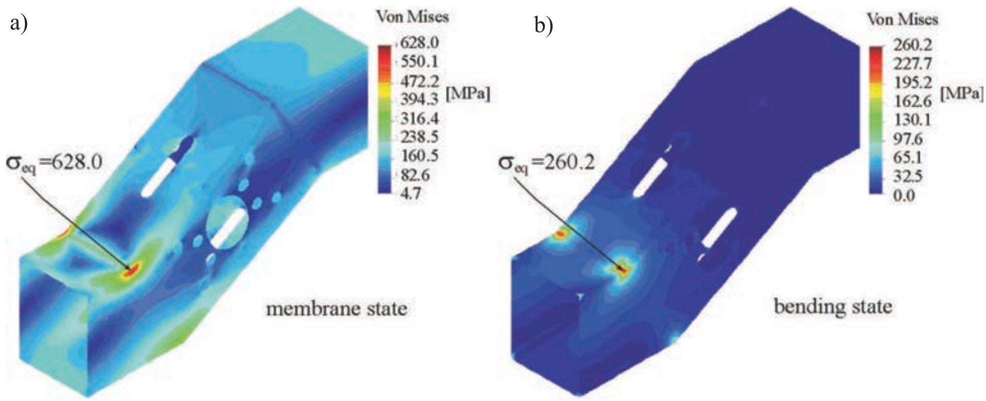

FIG. 3. Results of FEM analysis obtained for structural model with removed diaphragm.

4.2. Joint connecting bent sections of twin-tee and box types

The shapes of the analysed structure model, together with the assumed boundary conditions, are shown in Fig. 4a. Similarly as it was in the previ-

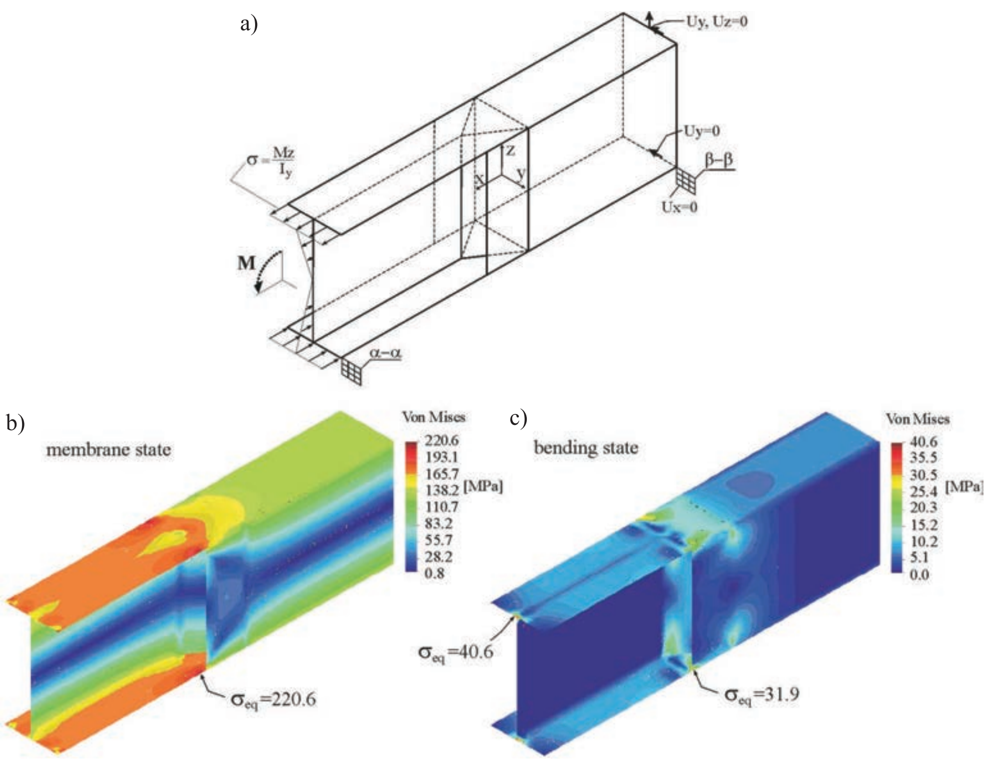

FIG. 4. Shapes and assumed boundary conditions of the analysed structure model as well as obtained distributions of equivalent stresses.

ous example, the load by a bending moment introduced in the cross-section α-α had a distribution consistent with beam-type distributions. The nodes lying in the cross-section β-β were deprived of the possibility of moving in the direction of the x axis. Additionally, one assumed displacements preventing the possibility of rigid motion.

Based on the results obtained in membrane state (Fig. 4b) one can conclude that, among other things:

- there appear harmful states associated with the axis of elastic bending;
- the level of effort is well equalised in the flanges of the structure;
- there appear low concentrations of stress locally, in the central part of flanges, where $\sigma_{\mathrm{eq}} = 220.6$ MPa.

The effort associated with bending state (Fig. 4c) is small, and maximal value of effort in this state reaches barely 14.5% of the values associated with membrane state (31.9/220.6).

4.3. Joint connecting torsional box-type section with bent section of twin-tee type

The boundary conditions and shapes of the structure model are well illustrated in Fig. 5a. The load by torsional moment was introduced in the plane α-α by means of shear forces of constant values around the whole circumference of

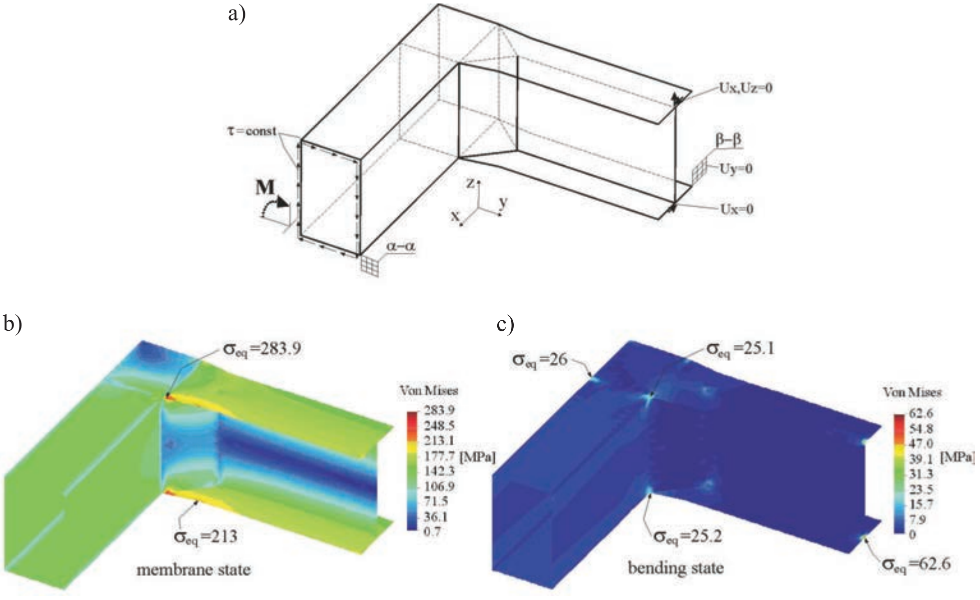

FIG. 5. Boundary conditions, shapes of the analysed structure model and obtained distributions of equivalent stresses.

the cross-section. The nodes lying in the cross-section β-β were deprived of the possibility of moving in the direction of the y axis. Additionally, one assumed displacements preventing the possibility of rigid motion.

In this case, one can conclude that in membrane state (Fig. 5b):

- the level of effort is ideally equalised in the torsional box section where pure shear load in the statically admissible stress field is assumed;
- the states characteristic for the bending axis are formed in the bent twin-tee section; equalisation of effort in the flanges of this section is good;
- local concentrations of stress in the vertices and corners of the structure are relatively low.

The effort asociated with bending state (Fig. 5c) reaches barely 10% of the values associated with membrane state (26/283.9).

5. Conclusions

In this study, the author presented a small fragment of FEM analyses carried out by him on thin-walled structures designed with the use of the SADSF method. In all cases – similarly as in the cases presented in this paper – one obtained good, and sometimes even very good load-carrying properties: domination of membrane states, low concentrations of stress and good equalization of elastic effort. Similar conclusions, based on investigations on elastic range pertaining to other cases of structure design, can be found in the whole literature of the subject [1, 3–12].

The results obtained so far allow us to confirm great practical usefulness of the SADSF method in designing thin-walled structures. The quality of stress fields realized in the systems designed in this way is absolutely incomparable to that obtained by using traditional methods.

Taking into account low level of bending forces, confirmed by the investigations, one can hardly expect large bending deformations in the exploitation range of load. However, in some fragments of certain structures, characterized by high slenderness ratio, the loss of stability at higher loads might be possible. The probability of maintaining the membrane state of stress up to the moment when limit load capacity is reached, as it is assumed in the SADSF method, seems to be low. However, as it results from investigations on other systems designed by this method, the assumed limit load capacity will most probably be obtained anyway [1, 4, 8].

The level of quality of preliminary designs of structures made by the SADSF method is good, so that these are worthy of expenses for further numerical analyses. In the cases of thin-walled structures, these systems are, first of all, free of structural errors, to which this class of structures is particularly sensitive, and the existence of which can deteriorate – even several dozens times – load carrying properties and global strength of the structure [1, 8]. The SADSF method eliminates such errors automatically. In contrast, the FEM makes it possible to notice such errors only after carrying out complete calculations, and even then it can not provide adequate hints of how to introduce the necessary corrections [1].

References

1. W. Bodaszewski, W. Szczepiński, *Shaping Structure Elements by the Method of Discontinuous Stress Fields* [in Polish], BEL Studio 2005, PWN, 2006.
2. W. Bodaszewski, *The software package KNPN for approximated shaping of complex plastic structures* [in Polish], VII-th Symposium on Stability of Structures, pp. 25–30, 1997.
3. W. Bodaszewski, I. Markiewicz, *Analysis of elastic effort in thin-walled open structures shaped by the method of statically admissible discontinuous stress fields* [in Polish], Conference Thin-Walled Vessels, pp. 7–10, Karłów 1998.
4. W. Bodaszewski, I. Markiewicz, *The investigation of shells shaped by the SADSF method in the full range of equilibrium paths* [in Polish], 19th Symposium on Experimental Mechanics of Solids, pp. 145–150, Jachranka 2000.
5. P. Gomoliński, *Computer aided design of structural elements with the use of the limit load capacity criterion* [in Polish], PhD thesis, Warsaw University of Technology, 1995.
6. I. Markiewicz, *Numerical analysis of elastic effort fields for the torsioned truss segment of jib shaped by the SADSF method* [in Polish], XIII Conference Problems of working machines development, vol. 2, pp. 17–22, Zakopane 2000.
7. I. Markiewicz, *Analysis of Elastic Effort Fields in Truck Frame Designed by the SADSF Method*, Maintenance and Reliability, 2 (34), 22–27, 2007.
8. I. Markiewicz, W. Bodaszewski, G. Glinka, *Global and Local Design Method for Fatigue Resistant Structures*, SAE 2003 Transactions, Journal of Materials and Manufacturing, Section 5 – **112**, 467–477, 2003.
9. W. Szczepiński, *Plastic design of machine parts* [in Polish], PWN, Warszawa 1968.
10. W. Szczepiński, L. Dietrich, *Plastic Design of Complex Shape Structural Elements – A Theoretical and Experimental Study*, pp. 1–8, Paryż 1981.
11. W. Szczepiński, J. Szlagowski, *Plastic Design of Complex Shape Structures*, Ellis Horwood & PWN, Warszawa – Chichester 1990.
12. J. Szlagowski, *Methodology of strength design of structural elements according to the limit load carrying capacity criterion* [in Polish], IFTR Reports, 25/1990.

Received June 4, 2008.

ENGINEERING TRANSACTIONS • Engng. Trans. • **57**, 1, 45–66, 2009
Polish Academy of Sciences • Institute of Fundamental Technological Research

NATURAL VIBRATION FREQUENCIES OF TAPERED BEAMS

M. A. De Rosa [1], M. Lippiello [2]

[1] **Faculty of Engineering**
Department of Structural Engineering, (DiSGG)
Viale dell'Ateneo Lucano, 10, 85100, Potenza, Italy

[2] **Faculty of Architecture**
Department of CoMMA
Via Forno Vecchio 36, 80134, Naples, Italy

In this paper the free vibrations frequencies of tapered Euler-Bernoulli beams are calculated, in the presence of an arbitrary number of rotationally and/or axially, elastically flexible constraints. The dynamic analysis is performed by means of the so-called cell discretization method (CDM), according to which the beam is reduced to a set of rigid bars, linked together by elastic sections, where the bending stiffness and the distributed mass of the bars is concentrated. The resulting stiffness matrix and mass matrix are easily deduced, and the generalized symmetric eingenvalue problem can be immediately solved. Various numerical comparisons allow us to show the potentialities of the proposed approach.

Key words: free vibrations, tapered beam, elastically restrained, CDM.

1. Introduction

The dynamic analysis of beams with continuously varying cross-section is a classical structural problem, which nowadays is becoming more and more important, even in mechanical engineering and in aeronautic engineering.

Numerous authors have approached the analysis assuming that the beam is sufficiently slender to be considered as an Euler-Bernoulli beam, and trying to analytically solve the resulting fourth-order differential equation with variable coefficients. Among the others, Craver and Jampala [1] examine the free vibration frequencies of a cantilever beam with variable cross-section and constraining springs; De Rosa and Auciello [2] give the exact free frequencies of a beam with linearly varying cross-section, in the presence of generic non-classically boundary conditions, so that all the usual boundary conditions can be treated as particular cases; Datta and Sill [3] give the general solution in terms of Bessel functions, and the first eingevalue for a beam with constant width and linearly varying height is found. In 1995 Abrate [4] solved the differential equation for various taper laws, and also performed a numerical comparison with the

Rayleigh–Ritz approach. Grossi *et al.* [5] employed both the classical Rayleigh–Ritz method and the optimized Rayleigh–Schmidt method to find the frequencies of beams with constant width and varying height, and also of beams with varying width and varying height. A lot of numerical results were given, for various non-classical boundary conditions. Mou *et al.* [6] employed the exact dynamic stiffness matrix (EDSM) to find the frequencies of circular and elliptic tapered beams, and of beams defined by a linear-tapered section, a uniform section and a non-linearly varying section. All the results are compared with a classical finite element analysis. The Rayleigh–Ritz approach is used by Zhou and Cheung [7] to find the first free vibration frequencies of three different tapered beams with various boundary conditions and truncation factors. Finally, free vibrations of Euler-Bernoulli beams of bilinearly varying thickness are studied in [8] using: a) the optimized Rayleigh–Ritz method, b) the differential quadrature technique and c) the finite element approach.

Tapered beams with more complex geometry and non-classical boundary conditions were studied by Auciello *et al.* in [9–10]; the beam is divided into two segments, and each segment has a different tapering law. The exact solutions are obtained in both the above-mentioned papers, solving the corresponding boundary value problem.

In [11–14] the dynamic stability problem of a non-prismatic beam is solved using the Chebyshev series approximation: the method is used to solve the problem of vibration for a Euler–Bernoulli and Timoshenko beams.

In this paper a numerical approach is adopted, to find the free vibration frequencies of Euler–Bernoulli multi-span beams with arbitrarily varying cross-sections, in the presence of elastically flexible supports. The analysis is performed reducing the beam to a set of rigid bars linked together by means of elastic sections (elastic cells), in which the stiffness and the mass of the beam is properly concentrated. In this way, the structure is reduced to a system with finite number of degrees of freedom, and the global stiffness matrix and the global mass matrix can be easily calculated. Obviously, the method can be dated back to the first manual attempts to solve the vibration problem [15–16 e.g.], but in this paper its feasibility to be computerized is clearly shown, using the powerful symbolic software *Mathematica* [17], and various numerical comparisons show the method's usefulness.

2. Formulation of the problem

Let us consider the beam in Fig. 1, with span L, Young modulus E and mass density ρ, resting on elastically flexible constraints at the ends, with rotational stiffness k_{RL} at left and k_{RR} at rigth, and axial stiffness k_{TL} at left and k_{TR} at rigth, respectively.

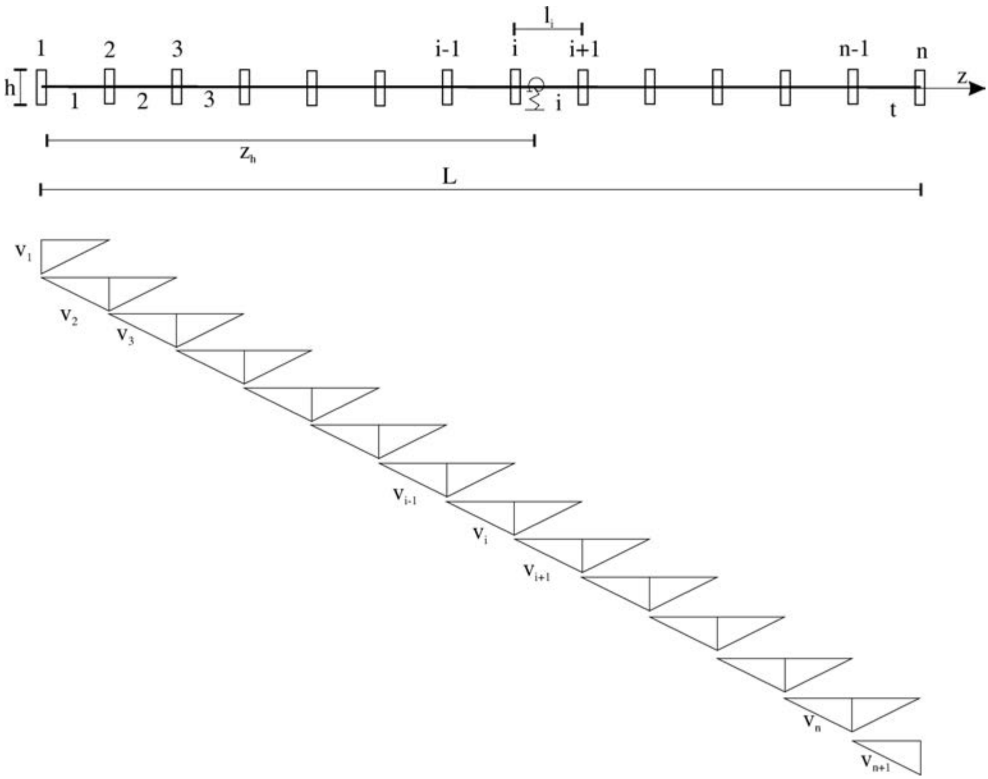

FIG. 1. Structural system.

Moreover, let us suppose that both the moment of inertia $I(z)$ and the cross-sectional area $A(z)$ vary with the abscissa z. As already said, the beam is reduced to a set of t rigid bars with length l_i, connected by $n = t + 1$ elastic cells. Whereas the possibility to adopt different lengths for each bar is invaluable in order to simulate rapidly varying geometries, nevertheless in the following we shall adopt the simplest choice, for which, $l_i = l, \ i = 1, ...t$. Moreover, the moment of inertia $I(z)$ and the cross-sectional area $A(z)$ will be evaluated at the cells abscissae, obtaining the concentrated stiffness $k_i = EI(z)/l$ and the concentrated masses $m_i = \rho A(z)l$. Both these quantities can be organized into the so-called unassembled stiffness matrix $\mathbf{k} = \mathrm{diag}\{k_i\}, \ i = 1, ...n$ and the unassembled mass matrix $\mathbf{M} = \mathrm{diag}\{m_i\}, \ i = 1, ...n$.

In this way, the structures is reduced to a classical holonomic system, with n degrees of freedom. The n vertical displacements v_i at the cells abscissae can be assumed as Lagrangian coordinates, and they will be organized into the n-dimensional vector $\mathbf{v}$; equivantely, the vector $\mathbf{v}$ can be viewed as a $(n\times1)$-dimensional matrix. The $n - 1$ rotations of the rigid bars can be calculated as a function of the Lagrangian coordinates as follows:

$$\phi_i = \frac{v_{i+1} - v_i}{l} \tag{2.1}$$

or, in matrix form: $\phi = \mathbf{V}\mathbf{v}$ and $\mathbf{V}$ is a rectangular transfer matrix with $n-1$ rows and n columns.

The relative rotations between the two faces of the elastic cells are given by:

$$\psi_1 = \phi_1, \qquad \psi_i = \phi_i - \phi_{i-1}, \qquad \psi_n = -\phi_{n-1}, \tag{2.2}$$

or in matrix form $\psi = \Delta\phi$, and Δ is another rectangular transfer matrix with n rows and $n-1$ columns.

The bending strain energy L_e is concentrated at the cells, and is given by:

$$L_e = \frac{1}{2}\sum_{i=1}^{n} k_{ii}\,\psi_i^2 = \frac{1}{2}\boldsymbol{\psi}^T\mathbf{k}\boldsymbol{\psi}. \tag{2.3}$$

In order to obtain a quadratic form of the Lagrangian coordinates it is necessary to use Eqs. (2.1)–(2.2):

$$L_e = \frac{1}{2}\boldsymbol{\psi}^T\mathbf{k}\boldsymbol{\psi} = \frac{1}{2}\boldsymbol{\phi}^T\Delta^{\mathrm{T}}\mathbf{k}\,\Delta\boldsymbol{\phi} = \frac{1}{2}\mathbf{v}^T\left(\mathbf{V}\Delta^{\mathrm{T}}\mathbf{k}\Delta\mathbf{V}\right)\mathbf{v} \tag{2.4}$$

or else:

$$L_e = \frac{1}{2}\mathbf{v}^T\mathbf{K}\mathbf{v}, \tag{2.5}$$

where $\mathbf{K}$ is the assembled stiffness matrix.

The kinetic energy can be simply expressed as:

$$T = \frac{1}{2}\mathbf{v}^T\mathbf{M}\mathbf{v}. \tag{2.6}$$

The strain energy of the axially flexible constraints at the ends is given by:

$$L_{TL} = \frac{1}{2}k_{TL}v_1^2, \qquad L_{TR} = \frac{1}{2}k_{RL}v_n^2, \tag{2.7}$$

so that the assembled stiffness matrix must be modified as follows:

$$K[1,1] = K[1,1] + k_{TL}, \qquad K[n,n] = K[n,n] + k_{TR}. \tag{2.8}$$

The presence of axially flexible intermediate supports can be similarly dealt with. If the constraint is placed at the abscissa $z_h = z_i + l_h$, and if its axial stiffness is given by k_T, its vertical displacement is given by (cf. Fig. 2):

$$v_h = v_i + \frac{v_{i+1} - v_i}{l}l_h \tag{2.9}$$

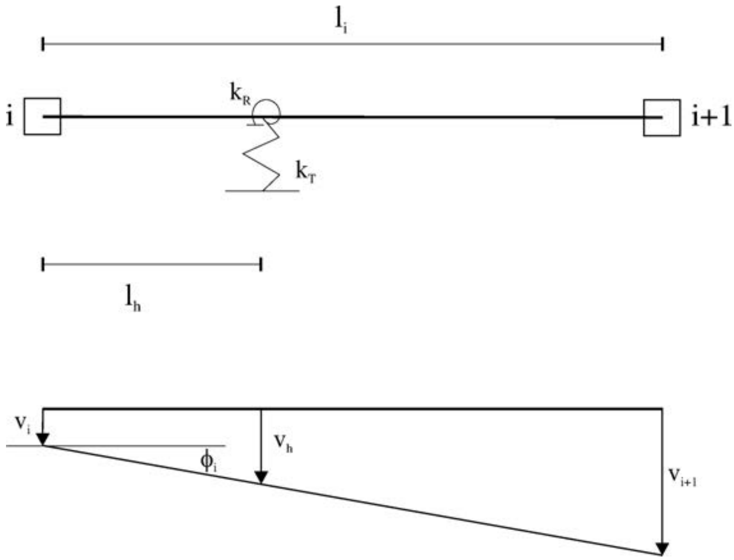

FIG. 2. Intermediate axially and rotationally flexible supports.

and its strain energy is equal to:

$$L_T = \frac{1}{2} k_T v_h^2. \tag{2.10}$$

The rotational stiffnesses of the constraints can be taken into account by summing up the corresponding flexibilities with the flexibilities of the rigid bars. For example, for the end constraints we have:

$$K[1,1] = \frac{K[1,1]\,k_{RL}}{k_{RL} + K[1,1]}, \qquad K[n,n] = \frac{K[n,n]\,k_{RR}}{k_{RR} + K[n,n]}. \tag{2.11}$$

The equation of motion can be written as:

$$\mathbf{M}\ddot{\mathbf{v}} + \mathbf{K}\mathbf{v} = \mathbf{0}. \tag{2.12}$$

The resulting generalized symmetric eingevalue problem can be easily solved, and the frequencies ω_i^2 can be obtained, together with the corresponding vibration modes.

3. Numerical comparisons

In order to show the method's potentialities, several numerical examples will be examined, using a general code developed in *Mathematica* [17]. In this paper we are not particularly interested in the convergence properties of the solutions, therefore all the examples will be performed by using a large number of cells, i.e. $n = 300$.

1. As a first numerical comparison, let us consider a tapered Euler-Bernoulli beam with cross-sectional area and moment of inertia given by the following laws:

$$A(z) = A_0\left((\alpha-1)\frac{z}{L}+1\right)^2, \qquad I(z) = I_0\left((\alpha-1)\frac{z}{L}+1\right)^4, \tag{3.1}$$

where $\alpha = \dfrac{h_1}{h_0} = \dfrac{b_1}{b_0}$, and A_0 and I_0 are the cross-sectional area and the moment of inertia of the section at left.

The beam is constrained at both ends with elastically flexible constraints, defined by the following non-dimensional quantities:

$$R_1 = \frac{k_{RL}L}{EI_0}, \qquad R_2 = \frac{k_{RR}L}{EI_1}, \qquad T_1 = \frac{k_{TL}L^3}{EI_0}, \qquad T_2 = \frac{k_{TR}L^3}{EI_1}. \tag{3.2}$$

This structure has been already solved in [2] using an exact approach, and the first five non-dimensional frequencies $p_i = \sqrt{\sqrt{\dfrac{\rho A_0 \omega_i^2 L^4}{EI_0}}}$ are reported in Table 1. With this discretization level, the discrepancies are negligible.

Table 1. Numerical comparison between the first five non-dimensional frequency coefficients p_i for $T_1 = T_2 \to \infty$, $\alpha = 2$.

R_1	R_2	p_1	p_2	p_3	p_4	p_5
0	0	3.7300 3.7300	7.6302 7.6301	11.4217 11.4212	15.2083 15.2072	18.9954 18.9932
0	0.01	3.7345 3.7345	7.6317 7.6316	11.4226 11.4221	15.2089 15.2078	18.9959 18.9937
0	0.1	3.7737 3.7737	7.6447 7.6446	11.4306 11.4301	15.2147 15.2136	19.0004 19.9982
0	1	4.0635 4.0635	7.7619 7.7618	11.5054 11.5049	15.2695 15.2684	19.0436 19.0114
0	10	4.7549 4.7549	8.2846 8.2845	11.9277 11.9272	15.6221 15.6209	19.3456 19.3432
1	0	3.7984 3.7984	7.6803 7.6802	11.4604 11.4600	15.2397 15.2386	19.0218 19.0195
1	0.1	3.8409 3.8409	7.6946 7.6945	11.4693 11.4688	15.2461 15.2450	19.0267 19.0245
1	1	3.1249 3.1249	7.8105 7.8104	11.5436 11.5431	15.3007 15.2995	19.0698 19.0676

2. The free vibration frequencies of cantilever tapered beams have been studied by Abrate [4] using a Rayleigh–Ritz approach and an n-term approximation.

The non-dimensional frequencies $\Omega_i = \omega_i \sqrt{\dfrac{\rho A_0 L^4}{E I_0}}$ are given in Table 2, for the following variation law:

$$\frac{A}{A_0} = \frac{I}{I_0} = 1 + \alpha z. \tag{3.3}$$

Table 2. First four non-dimensional frequency coefficients Ω_i for $\alpha = 0$ and $\alpha = -1/2$.

α	N	Mode	Abrate [4]	Hodges [19]	Thomson [18]	CDM
0	10	1	3.5160152	–	3.5160	3.5160
$-1/2$	10	1	4.3151703	4.3151703	–	4.3151575
		2	23.519257	–	–	23.518686
		3	63.199197	–	–	63.195723
		4	122.43963	–	–	122.42584

In the same table, the exact values for a constant beam are reported from Thomson [18], as well as the particular case $\alpha = -\frac{1}{2}$, which was studied by Hodges [19] using a finite element transfer matrix approach.

The non-dimensional frequencies Ω_i are given in Table 3, for the following quadratic variation law:

$$\frac{A}{A_0} = \frac{I}{I_0} = 1 + z + z^2, \tag{3.4}$$

the Rayleigh–Ritz results have been obtained using 20 trial functions, and the results show some discrepancies within the sixth decimal place.

Table 3. As in Table 2, but $A/A_0 = I/I_0 = 1 + z + z^2$.

Mode	Abrate [4]	Hodges [19]	CDM
1	2.4707858401571	2.4707858401571	2.4707660120
2	19.844681725047	–	19.844038124
3	59.7740637	–	59.770332125
4	119.040848	–	119.02840258

3. A numerical comparison is illustrated in Table 4, between the results given by our approach and the results given by Grossi *et al.* [5], using a classical Rayleigh–Ritz method and a more sophisticated Rayleigh–Schmidt procedure.

Table 4. Numerical comparison between the results in [5] and CDM.

$\sqrt{\lambda_1}$				
R_1	$b_2/b_1 = 1$	$b_2/b_1 = .5$	$b_2/b_1 = 1$	$b_2/b_1 = .5$
	$T_2 = 0.00$		$T_2 = 0.10$	
0.0	–	–	0.32193	0.30080
	–	–	0.32172	0.30049
	–	–	0.32172	0.30046
0.1	0.90219	1.00180	0.90603	1.00401
	0.90200	1.00150	0.90574	1.00361
	0.90197	1.00145	0.90570	1.00355
10	1.95338	2.15046	1.95429	2.15123
	1.94044	2.13050	1.94110	2.13095
	1.93828	2.12654	1.93890	2.12696
100	2.05048	2.25019	2.05136	2.25095
	2.03481	2.22614	2.03544	2.2269
	2.03200	2.22101	2.03259	2.22141
∞	2.06219	2.26179	2.06306	2.26254
	2.04655	2.23784	2.04718	2.23828
	2.04367	2.23258	2.04427	2.23299
	$T_2 = 10$		$T_2 = \infty$	
0.0	1.06415	1.02179	2.36301	2.34082
	1.01514	0.95216	2.32154	2.27992
	1.00992	0.94413	2.31286	2.26429
0.1	1.19009	1.21458	2.39812	2.38694
	1.15137	1.16844	2.35653	2.32640
	1.14723	1.16320	2.34785	2.31092
10	2.04639	2.23125	3.10163	3.21538
	2.00323	2.17527	3.03750	3.12459
	1.99724	2.16623	3.02511	3.10289
100	2.13995	2.32944	3.27145	3.39476
	2.09525	2.27026	3.19917	3.29240
	2.08847	2.25981	3.18515	3.26755
∞	2.15052	2.33995	3.29341	3.41670
	2.10664	2.28179	3.22144	3.31473
	2.09989	2.27131	3.20739	3.28980

The example refers to a tapered beam resting on elastically flexible ends with axial stiffnesses T_1 and T_2 and rotational stiffnesses R_1 and R_2, respectively. The cross-sectional area and the moment of inertia vary according to the following laws:

$$A(z) = b(z)h(z) = A_1\left(1 + c_2\frac{z}{L}\right)\left(1 + c_1\frac{z}{L}\right), \tag{3.5}$$

$$I(z) = \frac{b(z)h(z)^3}{12} = I_1\left(1 + c_2\frac{z}{L}\right)\left(1 + c_1\frac{z}{L}\right)^3, \tag{3.6}$$

where $c_1 = \dfrac{h_2}{h_1} - 1$, $c_2 = \dfrac{b_2}{b_1} - 1$ and $A_1 = b_1h_1$, $I_1 = \dfrac{b_1h_1^3}{12}$ are the area and the moment of inertia of the initial section.

The first non-dimensional frequency $\sqrt{\lambda_1} = \sqrt{\sqrt{\dfrac{\rho A_1\omega_i^2L^4}{EI_1}}}$ is given in the Table 4 for $R_2 = 0$, $T_1 = \infty$, $\dfrac{h_2}{h_1} = 0.25$, and for various R_1 values. The first $\sqrt{\lambda_1}$ value has been obtained using the Rayleigh–Ritz method, the second value is obtained by the optimized Rayleigh–Schmidt method, and finally the last value has been obtained using the CDM. As expected, our values are nearer to the Rayleigh–Schmidt results.

4. The free vibration frequencies of tapered beams with circular or elliptic cross-sections have been studied by Mou *et al.* [6], using the exact dynamic stiffness matrix (EDSM). The variation laws of cross-sectional area and moment of inertia are given by:

$$A(z) = A_0\left(\frac{z}{L}\right)^n, \qquad I(z) = I_0\left(\frac{z}{L}\right)^m, \tag{3.7}$$

where A_0 and I_0 are the area and the moment of inertia of the largest cross-section, and m, n, are positive numbers.

Two particular cases are dealt with in some detail:

a) Circular cross-section with $n = 2p$, $m = 4p$ and $0.1 < p < 1$.

The first two non-dimensional frequencies $\lambda_i = \sqrt{\sqrt{\dfrac{\rho A_0\omega_i^2L^4}{EI_0}}}$ are given in Table 5 according to the EDSM, FEM and CDM, respectively, for a truncation factor $c = 0.4$.

b) Elliptic cross-section $n = p_1 + p_2$, $m = p_1 + 3p_2$, $c = 0.3$ and $p_1 = 0.3, 0.7$, $0.1 < p_2 < 1$.

As in Table 5, three sets of results are reported in Table 6, and in both the cases the CDM is nearer to the EDSM results than to the FEM results.

Table 5. Numerical comparison between the results in [6] and CDM. Circular cross-section.

$c = 0.4$						
	EDSM		FEM		CDM	
p	1st	2nd	1st	2nd	1st	2nd
0.1	3.19015	7.77380	3.21524	7.82701	3.19014	7.77367
0.2	3.25449	7.72284	3.27964	7.78458	3.25448	7.72272
0.3	3.31808	7.67068	3.34343	7.74074	3.31806	7.67056
0.4	3.38074	7.61739	3.40649	7.69554	3.38074	7.61727
0.5	3.44013	7.56198	3.46866	7.64903	3.44238	7.56291
0.6	3.50282	7.50765	3.52984	7.60125	3.50285	7.50755
0.7	3.56203	7.45133	3.58987	7.55227	3.56201	7.45123
0.8	3.61971	7.39411	3.64862	7.50211	3.61971	7.39402
0.9	3.67580	7.33606	3.70594	7.45084	3.67580	7.33597
1.0	3.73014	7.27722	3.76168	7.39850	3.73015	7.27714

Table 6. Numerical comparison between the results in [6] and CDM. Elliptic cross-section.

					EDSM		FEM		CDM	
c	p_1	p_2	m	n	1st	2nd	1st	2nd	1st	2nd
0.3	0.3	0.1	0.6	0.4	2.84831	6.73501	2.86186	6.77346	2.84830	6.73490
		0.2	0.9	0.5	2.87311	6.64825	2.88832	6.69790	2.87308	6.64810
		0.3	1.2	0.6	2.89672	6.56054	2.91376	6.62116	2.89672	6.56040
		0.4	1.5	0.7	2.91913	6.47194	2.93813	6.54326	2.91913	6.47182
		0.5	1.8	0.8	2.94029	6.38252	3.96133	6.46426	2.94023	6.38239
		0.6	2.1	0.9	2.95981	6.29231	2.98329	6.38421	2.95995	6.29220
		0.7	2.4	1.0	2.97812	6.20140	3.00393	6.30315	2.97819	6.20129
		0.8	2.7	1.1	2.99487	6.10984	3.023315	6.22114	2.99487	6.10973
		0.9	3.0	1.2	3.00852	6.01735	3.04087	6.13824	3.00990	6.01761
		1.0	3.3	1.3	3.02317	5.92507	3.05699	6.05451	3.02317	6.92498
	0.7	0.1	1.0	0.8	3.04548	6.90106	3.04583	6.91263	3.04541	6.88970
		0.2	1.3	0.9	3.06963	6.80113	3.07191	6.83524	3.06957	6.80099
		0.3	1.6	1.0	3.09245	6.71148	3.09686	6.75666	3.09246	6.71135
		0.4	1.9	1.1	3.11389	6.62094	3.12061	6.67692	3.11399	6.62082
		0.5	2.2	1.2	3.13410	6.52956	3.14308	6.59607	3.13410	6.52945
		0.6	2.5	1.3	3.15268	6.43741	3.16418	6.51415	3.15268	6.43730
		0.7	2.8	1.4	3.16966	6.34453	3.18383	6.43122	3.16966	6.34443
		0.8	3.1	1.5	3.1894	6.25100	3.20193	6.34732	3.18495	6.25091
		0.9	3.4	1.6	3.19843	6.15689	3.21839	6.26251	3.19844	6.15680
		1.0	3.7	1.7	3.21003	6.06266	3.23311	6.17686	3.21004	6.06217

5. The same structure has been studied by ZHOU *et al.* [7] for the particular case $n = 2$ and $m = 4$. The non-dimensional frequency coefficients $\Omega_i = \sqrt{\rho A_0 \omega_i^2 L^4 / EI_0}$ are given for various values of the truncation factor α, see Table 7, as obtained by the following five approaches:

a) Orthogonally generated polynomials as trial functions in the Rayleigh–Ritz energy approach [7], and 8 terms.
b) Generated polynomials as trial functions in the Rayleigh–Ritz method [20].
c) Exact solution [21].
d) Frobenius method [22].
e) CDM.

Table 7. Numerical comparison between the results in [7] and CDM.

α	Ref.	Ω_1	Ω_2	Ω_3	Ω_4	Ω_5
0.2	(a)	6.1664	18.385	39.834	71.245	112.89
	(b)	6.1964	18.386	39.837	71.288	113.33
	(c)	6.1964	18.385	39.834	71.242	112.83
	(d)	6.1914	18.386	39.834	–	–
	(e)	6.1964	18.385	39.834	71.235	112.81
0.5	(a)	4.6252	19.548	48.579	91.816	149.43
	(c)	4.6252	19.548	48.579	91.813	149.39
	(d)	4.6252	19.548	48.579	–	–
	(e)	4.6252	19.548	48.577	91.806	149.37
0.8	(a)	3.8551	21.057	56.630	109.76	180.66
	(c)	3.8551	21.057	56.630	109.76	180.61
	(e)	3.8551	21.056	56.627	109.75	180.58

6. Let us consider now a set of assembled tapered beams, as given for example by MOU *et al.* [6]. The structure is given by a linearly tapered beam, an uniform beam and a non-uniform tapered beams assembled together. The first three non-dimensional frequencies are given in Table 8, and even in this case we observe the excellent agreement with the EDSM results.

7. Another interesting case is examined by LAURA *et al.* in [8]. The structure has rectangular cross-section and constant width. In the first span the height is supposed to vary according to the following linear law:

$$h(z) = h_0 \left(1 - \alpha \frac{z}{L}\right), \qquad 0 \leq z \leq L_1, \tag{3.8}$$

whereas in the second midspan the height has a constant value, given by:

$$h(z) = h_0 \left(1 - \alpha \frac{L_1}{L}\right), \qquad L_1 \leq z \leq L. \tag{3.9}$$

Table 8. Numerical comparison between the results in [6] and CDM. Three-segment beam with a linear segment, a constant segment and non-linear segment.

	EDSM			FEM			CDM		
p	1st	2nd	3rd	1st	2nd	3rd	1st	2nd	3rd
0.1	0.98852	2.37379	3.83817	0.89936	2.15550	3.52085	0.98851	2.37373	3.83795
0.2	1.01947	2.40456	3.84090	0.92184	2.18313	3.53005	1.01946	2.40450	3.84070
0.3	1.04900	2.43651	3.84342	0.94309	2.21167	3.53950	1.04899	2.43646	3.84323
0.4	1.07703	2.46952	3.84568	0.96310	2.24096	3.54919	1.07702	2.46948	3.84551
0.5	1.10239	2.50353	3.84717	0.98185	2.27079	3.55908	1.10351	2.50338	3.84747
0.6	1.28844	2.53801	3.84915	0.99936	2.30097	3.56913	1.12843	2.53798	3.84902
0.7	1.15180	2.57311	3.85015	1.01566	2.33129	3.57925	1.15179	2.57309	3.86004
0.8	1.17364	2.60850	3.85045	1.03080	2.36155	3.58930	1.17364	2.60849	3.85040
0.9	1.19402	2.64396	3.85059	1.04484	2.39154	3.59912	1.19401	2.64395	3.85055
1.0	1.21300	2.67923	3.85084	1.05784	2.42108	3.60849	1.21299	2.67927	3.85080

The first three non-dimensional frequencies Ω_i are calculated as in the Example 5, and A_0 and I_0 are the area and the moment of inertia of the initial section. The simply supported beam and the clamped-clamped beam are examined in the Tables 9–10, where the results obtained by the Differential Quadrature Method

Table 9. Numerical comparison between four different discretization methods, for simply supported two-segment beam. The first three non-dimensional frequencies are given for various values of α and $\gamma = L_1/L$.

		$\alpha = 0.1$			$\alpha = 0.2$			$\alpha = 0.3$		
γ		Ω_1	Ω_2	Ω_3	Ω_1	Ω_2	Ω_3	Ω_1	Ω_2	Ω_3
0.25	(1)	9.629	38.56	86.84	9.387	37.64	84.86	9.145	36.72	82.87
	(2)	9.777	–	–	9.681	–	–	9.584	–	–
	(3)	9.627	–	–	9.388	–	–	9.143	–	–
	(4)	9.628	38.56	86.85	9.387	37.64	84.87	9.145	36.72	82.89
0.5	(1)	9.447	37.99	85.42	9.018	36.49	81.00	8.583	34.97	78.54
	(2)	9.733	–	–	9.577	–	–	9.404	–	–
	(3)	9.447	–	–	9.037	–	–	8.612	–	–
	(4)	9.446	37.99	85.43	9.018	36.49	82.01	8.583	34.97	78.55
0.75	(1)	9.374	37.56	84.59	8.863	35.62	80.29	8.331	33.64	75.91
	(2)	9.525	–	–	9.163	–	–	8.773	–	–
	(3)	9.382	–	–	8.870	–	–	8.338	–	–
	(4)	9.374	37.56	84.60	8.862	35.62	80.20	8.331	33.64	75.92

Table 10. Numerical comparison between four different discretization method, for clamped-clamped two-segment beam. The first three non-dimensional frequencies are given for various values of α and $\gamma = L_1/L$.

		$\alpha = 0.1$			$\alpha = 0.2$			$\alpha = 0.3$		
γ		Ω_1	Ω_2	Ω_3	Ω_1	Ω_2	Ω_3	Ω_1	Ω_2	Ω_3
0.25	(1)	22.000	60.46	118.38	21.625			21.250		
	(2)	22.059	–	–	21.729	–	–	21.383	–	–
	(3)	22.005	–	–	21.635	–	–	21.266	–	–
	(4)	22.000	60.46	118.42	21.625	59.25	115.92	21.250	58.04	113.41
0.5	(1)	21.675	59.55	116.48	20.971	57.41	112.03	20.262	55.25	107.52
	(2)	21.979	–	–	21.567	–	–	21.134	–	–
	(3)	21.681	–	–	20.985	–	–	20.287	–	–
	(4)	21.675	59.56	116.50	20.971	57.42	112.04	20.261	55.25	107.54
0.75	(1)	21.432	58.89	115.31	20.471	56.06	109.65	19.488	53.16	103.85
	(2)	21.507	–	–	20.641	–	–	19.778	–	–
	(3)	21.435	–	–	20.476	–	–	19.497	–	–
	(4)	21.432	58.90	115.35	20.471	56.06	109.68	19.488	53.17	103.88

(DQM), the optimized Rayleigh–Ritz method and the Finite Element Method (FEM) are compared with the CDM results. Even in this case, our results give an excellent lower bound.

8. A similar structure has been studied in [10], where the free vibration frequencies of a two-beam structure on flexible supports are exactly calculated. The first beam constant has a cross-section, the second beam is defined by the following taper law:

$$A(z) = A_1\eta^n, \qquad I(z) = I_1\eta^{n+2}, \tag{3.10}$$

with:

$$\eta\left[1 + \frac{\alpha - 1}{L(1-\beta)}z\right], \tag{3.11}$$

and β is a multiplying factor of the span of the first beam, $\alpha = \dfrac{h_2}{h_1}$, $\dfrac{b_2}{b_1} = 1$ and A_1, I_1 are the cross-sectional area and the moment of inertia of the initial section.

For a clamped-clamped beam, the first five free non-dimensional vibration frequencies $p_i = \sqrt{\sqrt{\dfrac{\rho A_1 \omega_i^2 L^4}{EI_1}}}$ are given in Tables 11–12 for various β and α values, as obtained using an exact approach and our discretization method.

Table 11. Numerical comparison between the results in [9] and CDM. Two-segment beam β=0 and β=0.2.

α	$\beta = 0$					$\beta = 0.2$				
	p_1	p_2	p_3	p_4	p_5	p_1	p_2	p_3	p_4	p_5
1	4.73	7.8532	10.9956	14.1372	17.2788	–	–	–	–	–
	4.73	7.8529	10.9949	14.1358	17.2764	–	–	–	–	–
1.25	5.0098	8.3172	11.6449	14.9718	18.2988	4.9828	8.2468	11.5303	14.8165	18.1036
	5.0097	8.3168	11.6442	14.9703	18.2962	4.9827	8.2464	11.5290	14.8136	18.0985
1.43	5.1933	8.6210	12.0699	15.5179	–	–	–	–	–	–
	5.1946	8.6230	12.0724	15.5206	–	–	–	–	–	–
1.5	5.2636	8.7374	12.2325	15.7268	19.2213	5.2104	8.5986	12.0071	15.4214	18.8356
	5.2634	8.7370	12.2317	15.7253	19.2186	5.2103	8.5982	12.0057	15.4183	18.8307
1.54	5.3007	8.7988	12.3184	15.8373	–	–	–	–	–	–
	5.3021	8.8009	12.3210	15.8401	–	–	–	–	–	–
1.66	5.4215	8.9985	12.5975	16.1958	–	–	–	–	–	–
	5.4152	8.9879	12.5824	16.1759	–	–	–	–	–	–
1.75	5.4976	9.1242	12.7732	16.4215	20.0700	5.4186	8.9189	12.4404	15.9700	19.4973
	5.4975	9.1239	12.7724	16.4198	20.1671	5.4185	8.9185	12.4390	15.9669	19.4924
2	5.7159	9.4848	13.2769	17.0684	20.7145	5.6112	9.1246	12.8398	16.4741	20.1029
	5.7157	9.4844	13.2760	17.0666	20.8570	5.6111	9.2142	12.8384	16.4709	20.0982
2.25	5.9213	9.8238	13.7502	17.6761	21.6024	5.7910	9.4904	13.2118	16.9418	20.6627
	5.9211	9.8233	13.7492	17.6742	21.5992	5.7910	9.4899	13.2103	16.9386	20.6581
2.5	6.1159	10.1447	14.1981	18.2512	22.3047	5.9601	9.7498	13.5609	17.3789	21.1841
	6.1157	10.1412	14.1971	18.2492	22.3012	5.9600	9.7493	13.5594	17.3758	21.1796
2.75	6.3012	10.4501	14.6243	18.7983	22.9727	6.1199	9.9954	13.8907	17.7899	21.6727
	6.3010	10.4496	14.6232	18.7961	22.3691	6.1199	9.9950	13.8891	17.7867	21.6683
3	6.4785	10.7421	15.0317	19.3211	23.6112	6.2719	10.2293	14.2038	18.1780	22.1329
	6.4783	10.7416	15.0305	19.3189	23.6074	6.2719	10.2288	14.2022	18.1749	22.1286
4	7.1242	11.8048	16.5134	21.2222	25.9321	6.8185	11.0756	15.3250	19.5488	23.7544
	7.1240	11.8041	16.5119	21.2194	25.9275	6.8185	11.0751	15.3232	19.5459	23.7501
5	7.6947	12.7427	17.8202	22.8984	27.9780	7.2960	11.8213	16.2894	20.7025	25.1251
	7.6944	12.7419	17.8183	22.8951	27.9724	7.2960	11.8206	16.2876	20.6999	25.1205
10	9.9421	16.4342	22.9582	29.4844	36.0136	9.2302	14.7957	19.7536	24.8107	30.1851
	9.9412	16.4322	22.9544	29.4779	36.0034	9.2301	14.7949	19.7524	24.8078	30.1771

Table 12. Numerical comparison between the results in [9] and CDM. Two-segment beam β=0.4 and β=0.6.

α	$\beta = 0.4$					$\beta = 0.8$				
	p_1	p_2	p_3	p_4	p_5	p_1	p_2	p_3	p_4	p_5
1.25	4.9557	8.1761	11.4107	14.6498	17.9006	4.9355	8.1007	11.3025	14.4934	17.7072
	4.9556	8.1758	11.4100	14.6481	17.8979	4.9354	8.1003	11.3017	14.4917	17.7042
1.5	5.1583	8.4647	11.7714	15.0992	18.4409	5.1286	8.3130	11.5711	14.8030	18.0716
	5.1582	8.4643	11.7707	15.0976	18.4383	5.1285	8.3126	11.5702	14.8013	18.0684
1.75	5.3450	8.7264	12.0917	15.5022	18.9192	5.3117	8.5015	11.8086	15.0804	18.3887
	5.3449	8.7261	12.0910	15.5005	18.9166	5.3116	8.5011	11.8077	15.0786	18.3854
2	5.5203	8.9661	12.3812	15.8689	19.3490	5.4852	8.6737	12.0202	15.3335	18.6705
	5.5203	8.9657	12.3804	15.8671	19.3464	5.4851	8.6733	12.0192	15.3318	18.6671
2.25	5.6874	9.1869	12.6465	16.2057	19.7399	5.6491	8.8350	12.2099	15.5672	18.9256
	5.6873	9.1866	12.6457	16.2040	19.7373	5.6490	8.8346	12.2089	15.5654	18.9221
2.5	5.8481	9.3913	12.8926	16.5173	20.0994	5.8032	8.9891	12.3813	15.7842	19.1603
	5.8480	9.3910	12.8918	16.5155	20.0968	5.8031	8.9886	12.3803	15.7823	19.1567
2.75	6.0040	9.5812	12.1233	16.8069	20.4332	5.9473	9.1383	12.5373	15.9862	19.3793
	6.0039	9.5809	12.1225	16.8052	20.4304	5.9472	9.1379	12.5362	15.9843	19.3757
3	6.1559	9.7581	13.3414	17.0773	20.7456	6.0814	9.2844	12.6805	16.1745	19.5859
	6.1558	9.7578	13.3405	17.0755	20.7428	6.0813	9.2839	12.6793	16.1725	19.5822
4	6.7646	10.3592	14.1231	18.0024	21.8410	6.5221	9.8517	13.1664	16.8069	20.3242
	6.7345	10.3589	14.1221	18.0007	21.8377	6.5219	9.8513	13.1650	16.8046	20.3230
5	7.2772	10.8334	14.8061	18.7435	22.7672	6.8326	10.3908	13.5838	17.2834	20.9536
	7.2771	10.8331	14.8050	18.7417	22.7637	6.8323	10.3903	13.5824	17.2807	20.9495
10	9.4280	12.4761	17.2360	21.3717	25.8612	7.4616	12.0636	15.7599	22.7572	26.8834
	9.4279	12.4755	17.2349	21.3692	25.8572	7.4610	12.0623	15.7585	18.7567	22.7506

9. An interesting two-beams structure has been studied in [9], where the first beam is defined by the following taper ratio:

$$A(z) = A_1 \left[1 + \frac{\alpha_1 - 1}{\beta L} z\right]^n,$$

$$I(z) = I_1 \left[1 + \frac{\alpha_1 - 1}{\beta L} z\right]^{n+2}, \tag{3.12}$$

$$0 \le z \le \beta L,$$

whereas for the second beam we have:

$$A(z) = A_1 \left[\frac{\alpha_1\alpha_2 - \alpha_1}{L(1-\beta)}(z-L) + \alpha_1\alpha_2 \right]^n ,$$

(3.13)

$$I(z) = I_1 \left[\frac{\alpha_1\alpha_2 - \alpha_1}{L(1-\beta)}(z-L) + \alpha_1\alpha_2 \right]^{n+2}$$

and $\beta L \leq z \leq L$.

The structure is supposed to be clamped at left, and resting on an elastically flexible end at right.

The first three free non-dimensional frequencies p_i, as in Table 11, are given in Tables 13–14 for various β, α and various materials. Even in this last case, our results present an excellent lower bound.

10. The numerical example which is presented below was taken from Ref. [11]: in this paper, the problem of vibration of beam with rectangular cross-section, where the base is constant and the height is variable, was studied. In this case, the variation laws of cross-sectional area and moment of inertia are given by

$$A(z) = A_0 \left(\frac{z}{L}(\alpha - 1) + 1 \right) ,$$

(3.14)

$$I(z) = I_0 \left(\frac{z}{L}(\alpha - 1) + 1 \right)^3 ,$$

where A_0 and I_0 are the cross-sectional area and the moment of inertia of the initial beam, respectively, and $\alpha = h_2/h_1 = 0.5$, where h_1 and h_2 are the initial and final beam's cross-section height, respectively.

By using the data of the numerical example, p. 461 of the paper [11], the vibration frequencies are determined:

$$f_i = \frac{\omega_i}{2\pi}. \tag{3.15}$$

In particular, in Table 15 the first seven vibration frequencies for a simply supported beam (Example (a)) and the first five vibration frequencies for a cantilever beam (Example (b)) are reported.

The problem of vibration frequencies is solved using the presented method and the Chebyshev series approximation: the obtained results show an excellent agreement.

In Appendix 1 the numerical program, using "Mathematica" code, is reported. The data refer to this particular case, as can be noted by the cross-sectional areas and moment of inertia expressions which are identical to those of Formula (3.14).

Table 13. Numerical comparison between the results in [10] and CDM. Two-segment beam with the first constant segment and the second variable segment. Wedge beam.

$\alpha_1 = \alpha_2 = 1.5$				
	β	p_1	p_2	p_3
Single material $\varepsilon = 1$ $\nu = 1$	0.2	2.960984	6.623893	10.653342
		2.961004	6.623736	10.652826
	0.4	2.955257	6.339284	10.116494
		2.955256	6.339196	10.116103
	0.6	2.831723	6.092949	9.714487
		2.831713	6.092845	9.714025
	0.8	2.610069	5.874837	9.440699
		2.609593	5.874592	9.439987
Aluminium $\varepsilon = 3$ $\nu = 2.88889$	0.2	3.341329	7.266658	10.982127
		3.341349	7.626415	10.981648
	0.4	3.638804	6.379341	10.365182
		3.638802	6.379263	10.364734
	0.6	3.352323	6.436236	9.652822
		3.352308	6.436130	9.652349
	0.8	2.809352	6.321979	9.990769
		2.809358	6.321652	9.989850
Steel-Aluminium $\varepsilon = 0.33333$ $\nu = 0.34615$	0.2	2.448228	6.152010	10.232177
		2.448235	6.151898	10.231652
	0.4	2.310298	5.987174	10.093364
		2.310299	5.987064	10.092935
	0.6	2.255394	5.732798	9.537642
		2.255445	5.732686	9.537146
	0.8	2.258520	5.874837	9.440699
		2.258414	5.453477	9.047567
Tungsten-Aluminium $\varepsilon = 0.2$ $\nu = 0.15$	0.2	2.223087	6.381117	10.567467
		2.224018	6.380980	10.566875
	0.4	2.050444	5.865405	10.710794
		2.051179	5.865266	10.710309
	0.6	2.006496	5.539217	9.568246
		2.006565	5.539101	9.567671
	0.8	2.060400	5.308516	8.883911
		2.060452	5.308366	8.883313
Aluminium-Tungsten $\varepsilon = 5$ $\nu = 6.66666$	0.2	3.223087	7.139275	10.91989
		3.221416	7.138936	10.619406
	0.4	3.797734	6.077439	9.997253
		3.797706	6.077367	9.996747
	0.6	3.527982	6.354572	9.292952
		3.527960	6.354485	9.292463
	0.8	2.858571	6.472948	10.206816
		2.858605	6.472582	10.205816

Table 14. Numerical comparison between the results in [10] and CDM. Two-segment beam with the first constant segment and the second variable segment. Cone beam.

$\alpha_1 = \alpha_2 = 1.5$				
	β	p_1	p_2	p_3
Single material $\varepsilon = 1$ $\nu = 1$	0.2	3.241992	6.890704	10.872190
		3.241997	6.890536	10.871682
	0.4	3.295517	6.585544	10.284771
		3.295519	6.585466	10.284399
	0.6	3.135124	6.355970	9.883609
		3.135132	6.355880	9.883170
	0.8	2.826031	6.098033	9.655944
		2.826067	6.097798	9.655200
Aluminium $\varepsilon = 3$ $\nu = 2.88889$	0.2	3.601942	7.570925	11.289006
		3.601924	7.570652	11.288512
	0.4	4.013659	6.625189	10.579703
		4.013651	6.625127	10.579268
	0.6	3.653699	6.759004	9.818821
		3.653686	6.758905	9.8183760
	0.8	3.005513	6.525742	10.241486
		3.005487	6.525412	10.240488
Steel-Aluminium $\varepsilon = 0.33333$ $\nu = 0.34615$	0.2	2.719027	6.366531	10.431558
		2.719020	6.363403	10.431012
	0.4	2.591143	6.257891	10.208067
		2.591070	6.257762	10.207648
	0.6	2.5200643	5.982285	9.7002030
		7.520663	5.982184	9.6997084
	0.8	2.484248	5.647080	9.2249650
		2.484001	5.646931	9.224344
Tungsten-Aluminium $\varepsilon = 0.2$ $\nu = 0.15$	0.2	2.485453	6.604193	10.794795
		2.485391	6.604093	10.794207
	0.4	2.303951	6.171426	10.786371
		2.303799	6.171287	10.785913
	0.6	2.247777	5.799427	9.727984
		2.247773	5.799312	9.727416
	0.8	2.280355	5.486273	9.059468
		2.280369	5.486060	9.058860
Aluminium-Tungsten $\varepsilon = 5$ $\nu = 6.66666$	0.2	3.444017	7.392360	10.993261
		3.444000	7.392008	10.992690
	0.4	4.142424	6.344458	10.200137
		4.142405	6.344406	10.199647
	0.6	3.816945	6.688564	9.456933
		3.816922	6.688486	9.456470
	0.8	3.048076	6.658406	10.461855
		3.048054	6.658042	10.460753

Table 15. Numerical comparison between the results in [11] and CDM. Non-prismatic beam. Example (a) – a simply supported beam. Example (b) – a cantilever beam.

Example (a)	f_1	f_2	f_3	f_4	f_5	f_6	f_7	f_8
This paper	188.44	757.97	1703.89	3027.50	4728.90	6808.07	9264.89	12099.20
[11]	188.44	757.99	1703.97	3027.75	4729.39	6808.80	9286.04	12103.70
Example (b)								
This paper	85.66	455.80	121.55	2350.21	3864.60	5746.44		
[11]	85.66	455.80	1215.48	2349.93	3862.32	5752.45		

11. Finally, in a recent paper [23] the free vibration frequency of an isotropic beam have been found, for a variable cross-section with an exponential law:

$$
\begin{aligned}
A(z) &= A_0 e^{\delta z}, \\
I(z) &= I_0 e^{\delta z},
\end{aligned}
\tag{3.16}
$$

where δ is the non-uniformity parameter.

In Table 16 the free vibration frequencies given in Table 1, p. 82 of the paper [23], have been reproduced using CDM. The agreement is very good, both for simply supported beams and for clamped-clamped beams. On the contrary, the discrepancies for the first two free frequencies in cantilever beams are noticeable, both for $\delta = -1, -2$ and for $\delta = 1, 2$, so that we have reproduced the calculations, as described in [19], and the newly calculated results show an excellent agreement with the CDM.

Consequently, it seems that the values given in [23] are misprinted.

4. Conclusions

The free vibration frequencies of tapered beams are studied, for arbitrary variation laws of cross-sectional area and moments of inertia, in the presence of rotationally and axially flexible supports. The beam is viewed as a set of rigid bars linked together at discrete sections, in which stiffness and mass are concentrated, and the resulting system with finite number of degrees of freedom is so simple to analyze to permit a careful discretization, using a large number of rigid bars (in our case, 300 bars). Several examples are treated in some details, comparing exact and approximate results from the literature, and the proposed approach always gives excellent results.

Table 16. Numerical comparison between the results in [22].

$\lvert\delta\rvert$	Mode number	Natural frequencies									
		SS		CC		CF					
		C.D.M.	[22]	C.D.M.	[22]	C.D.M.	[22]	C.D.M.	[22]	C.D.M.	[22]
0	1	9.86960	9.86960	22.37319	22.37327			3.51602	3.51602		
	2	39.47829	39.47841	61.67226	61.67281			22.03439	22.03449		
	3	88.82578	88.82643	120.90151	120.90338			61.69665	61.69721		
	4	157.91159	157.91367	199.85470	199.85945			120.90003	120.90191		
	5	246.73503	246.74011	298.54551	298.55552			199.85478	199.85953		
						$\delta < 0$		exact	excat	$\delta > 0$	
1	1	9.77291	9.77291	22.51158	22.51167	4.73491	4.72298	4.73491	2.56534	2.56534	2.85833
	2	39.57024	39.57036	61.85913	61.85968	24.20173	24.20168	24.20181	20.03838	20.03827	20.03917
	3	88.96986	88.97052	121.10610	121.10799	63.86395	63.86448			59.87027	59.87084
	4	158.08211	158.08418	200.06937	200.07411	123.09607	123.09790			119.09669	119.09862
	5	246.92142	246.92650	298.76659	298.77661	202.06410	202.06876			198.06480	198.06964
2	1	9.48725	9.48725	22.93763	22.93771	6.26264	6.25877	6.26264	1.84057	1.84053	2.90893
	2	39.85219	39.85231	62.42217	62.42272	26.58351	26.58350	26.58359	18.17212	18.17202	18.17520
	3	89.40455	89. 40520	121.72084	121.72272	66.37398	66.37449			58.38808	58.38868
	4	158.59481	158.59689	200.71386	200.71860	125.68293	125.68471			117.69019	117.69217
	5	247.48121	247. 48629	299.43011	299.44012	204.69073	204.69531			196.69732	196.70224

Appendix 1

```
Cell1[n_, span_, h1_, h2_, b_, young_, ρ_, kTL_, kTR_, kRL_, kRR_] :=
    Module[
        {i, j, t, α, I0, A0, z, m, inerz, are, k, V, Δ, K, M, FREQUENCIES},
        t = (span)/(n - 1); α = h2/h1; I0 = b * h1^3/12; A0 = b * h1;
  z = Table[0, {i, 1, n}]; m = Table[0, {i, 1, n}];
  inerz = Table[0, {i, 1, n}]; are = Table[0, {i, 1, n}];
k = Table[0, {i, 1, n}, {j, 1, n}]; V = Table[0, {i, 1, n - 1}, {j, 1, n}];
  Δ = Table[0, {i, 1, n}, {j, 1, n - 1}]; K = Table[0, {i, 1, n}, {j, 1, n}];
  M = Table[0, {i, 1, n}, {j, 1, n}]; FREQUENCIES = Table[0, {i, 1, n}, {j, 1, n}];
  z[[1]] = 0; z[[n]] = span; Do[z[[i]] = (i - 1) * t, {i, 2, n - 1}];
  Do[are[[i]] = A0 * (z[[i]]/span (α - 1) + 1), {i, 1, n}];
Do[inerz[[i]] = I0 * (z[[i]]/span (α - 1) + 1)^3, {i, 1, n}];
  m[[1]] = ρ * are[[1]] * t/2; m[[n]] = ρ * are[[n]] * t/2;
  Do[m[[i]] = ρ * are[[i]] * t, {i, 2, n - 1}];
k[[1, 1]] = young * inerz[[1]]/(t/2); k[[n, n]] = young * inerz[[n]]/(t/2);
  k[[1, 1]] = k[[1, 1]]/(1 + k[[1, 1]]/kRL);
k[[n, n]] = k[[n, n]]/(1 + k[[n, n]]/kRR);
  Do[k[[i, i]] = young * inerz[[i]]/t, {i, 2, n - 1}];
Do[V[[i, i]] = -1/t; V[[i, i + 1]] = 1/t, {i, 1, n - 1}];
  Do[Δ[[i, i]] = 1; Δ[[i + 1, i]] = -1, {i, 1, n - 1}];
Do[M[[i, i]] = 1/m[[i]], {i, 1, n}];
  K = Transpose[V].Transpose[Δ].k.Δ.V;
K[[1, 1]] = K[[1, 1]] + kTL; K[[n, n]] = K[[n, n]] + kTR;
FREQUENCIES = Sqrt[Chop[N[Eigenvalues[M.K]]]]/(2 π);
                              Return[FREQUENCIES]];
```

References

1. L. Craver Jr., P. Jampala, *Transverse vibrations of a linearly tapered cantilever beam with constraining springs*, J. of Sound and Vibr, **166**, 521–529, 1993.

2. M. A. De Rosa, N. M. Auciello, *Free vibrations of tapered beams with flexible ends*, Comp. & Struct., **60**, 197–202, 1996.

3. A. K. Datta, S. N. Sil, *An analysis of free undamped vibration of beams of varying cross-section*, Comp. & Struct., **59**, 479–483, 1996.

4. S. Abrate, *Vibration of non-uniform rods and beams*, J. of Sound and Vibr., **185**, 703–716, 1995.

5. R. O. Grossi, B. del V. Arenas, *A variational approach to the vibration of tapered beams with elastically restrained ends*. J. of Sound and Vibr., **195**, 507–511, 1996.

6. Y. Mou, R. P. Han, A. H. Shah, *Exact dynamic stiffness matrix for beams of arbitrarily varying cross-sections*, Int. J. Num. Methods Engrg., **40**, 233–250, 1997.

7. D. Zhou, Y. K. Cheung, *The free vibrations of a type of tapered beams*, Comput. Methods Appl. Mech. Engrg., **188**, 203–216, 2000.

8. P. A. A. Laura, R. H. Gutierrez, R. E. Rossi, *Free vibrations of beams of bilinearly varying thickness*, Ocean Engrg, **23**, 1–6, 1996.

9. N. M. Auciello, G. Nolè, *Vibrations of a cantilever tapered beam with varying section properties and carrying a mass at the free end*, J. of Sound and Vibr., **214**, 105–119, 1998.

10. N. M. Auciello, A. Ercolano, *Exact solution for the transverse vibration of beam, a part of which is a taper beam and other part is a uniform beam*, Int. J. Solids Structures, **34**, 2115–2129, 1998.

11. P. Ruta, *Application of Chebyshev series to solution of non-prismatic beam vibration problems*, J. of Sound and Vibr., **227** (2), 449–467, 1999.

12. P. Ruta, *Dynamic stability problem of a non-prismatic rod*, J. of Sound and Vibr., **250** (3), 445–464, 2002.

13. P. Ruta, *The vibration of a non-prismatic beam on an inertial elastic half-plane*, J. of Sound and Vibr., **275**, 533–556, 2004.

14. P. Ruta, *The application of Chebyshev polynomials to the solution of the non-prismatic Timoshenko beam vibration problem*, J. of Sound and Vibr., **296**, 243–263, 2006.

15. M. A. De Rosa, *Stability and dynamics of beams on Winkler elastic foundations*, Earth. Engrg. Struct. Dyn., **18**, 377–388, 1989.

16. M. A. De Rosa, *Stability and dynamic analysis of two- parameter foundation beams*, Comp. & Struct., **49**, 341–349, 1993.

17. S. Wolfram, *The Mathematica Book*, 4rd edition, Wolfram Media Cambridge University Press, Cambridge, 1999.

18. W. T. Thomson, *Theory of vibration with applications*, Englewood Cliff, New Jersey, Prentice-Hall, (1972).

19. D. H. Hodges, Y. Y. Chung, X. Y. Shang, *Discrete transfer matrix method for non-uniform rotating beams*, J. of Sound and Vibr., **169**, 276–283, 1994.

20. C. S. Kim, S. M. Dickinson, *On the analysis of laterally vibrating slender beams to various complicating effects*, J. of Sound and Vibr, **122**, 441–455, 1988.

21. J. H. Lau, *Vibration frequencies of tapered bars with end mass*, ASME J. Appl. Mech., **51**, 179–181, 1984.

22. S. Naguleswaran, *A direct solution of Euler-Bernoulli wedge and cone beams*, J. of Sound and Vibr., **172**, 289-304, 1984.

23. M. C. Ece, M. Aydogdu, V. Taskin, *Vibration of a variable cross-section beams*, Mech. Res. Comm., **34**, 78–84, 2007.

Received July 4, 2008; revised version November 24, 2008.

DIRECTIONS FOR THE AUTHORS

The periodical *ENGINEERING TRANSACTIONS (ROZPRAWY INŻYNIERSKIE)* presents original papers which should not be published elsewhere.

As a rule, the volume of a paper should not exceed 40 000 typographic signs, that is about 20 type-written pages, format: 210×297 mm, leaded. The papers should be submitted in two copies and follow the norms outlined by the Editorial Office. The following directions are particularly important:

1. The paper submitted for publication should be written in English.
2. The title of the paper should be as short as possible. The text should be preceded by a brief introduction; it is also desirable that a list of notations used in the paper should be given.
3. Short papers should be divided into section and subsection, long papers into sections, subsections and points. Each section, subsection or point must bear a title.
4. The formula number consists of two figures: the first represents the section number and the other the formula number in that section. Thus the division into subsections does not influence the numbering of formulae. Only such formulae should be numbered to which the author refers throughout the paper. This also applies to the resulting formulae. The formula number should be written on the left-hand side of the formula; round brackets are necessary to avoid any misunderstanding. For instance, if the author refers to the third formula of the set (2.1), a subscript should be added to denote the formula, viz. $(2.1)_3$.
5. All the notations should be written very distinctly. Special care must be taken to distinguish between small and capital letters as precisely as possible. Semi-bold type must be underlined in black pencil. Explanations should be given on the margin of the manuscript in case of special type face.
6. Vectors are to be denoted by semi-bold type, transforms of the corresponding functions by tildes symbols. Trigonometric functions are denoted by sin, cos, tg and ctg, inverse functions – by arc sin, arc cos, arc tg and arc ctg; hyperbolic functions are denoted by sh, ch, th and cth, inverse functions – by Arsh, Arch, Arth and Arcth.
7. The figures in square brackets denote reference titles. Items appearing in the reference list should include the initials of the first name of the author and his surname, also the full of the paper (in the language of the original paper); moreover;
   a) In the case of books, the publisher's name, the place and year of publication should be given, e.g., 5. S. Ziemba, *Vibration analysis*, PWN, Warszawa 1970;
   b) In the case of a periodical, the full title of the periodical, consecutive volume number, current issue number, pp. from ... to ..., year of publication should be mentioned; the annual volume number must be marked in semi-bold type as to distinguish it from the current issue number, e.g., 6. M. Sokołowski, *A thermoelastic problem for a strip with discontinuous boundary conditions*, Arch. Mech., **13**, 3, 337–354, 1961.
8. The authors should enclose a summary of the paper. The volume of the summary is to be about 100 words.
9. The authors are kindly requested to enclose the figures prepared on diskettes (format WMF, EMF, GIF, PCX, BitMaP, EPS or PostScript).

Upon receipt of the paper, the Editorial Office forwards it to the reviewer. His opinion is the basis for the Editorial Committee to determine whether the paper can be accepted for publication or not.

Once the paper is printed, 25 copies of reprints free of charge are sent to the author.

The papers submitted for publication in the journal should be written in English. No royalty is paid to the authors.

Please send us, in addition to the typescript, the same text prepared on a diskette (floppy disk) 3 1/2″ as an ASCII file, preferably in the TEX or LATEX.

Editorial Committee
ENGINEERING TRANSACTIONS
(ROZPRAWY INŻYNIERSKIE)

ENGINEERING TRANSACTIONS **Appears since 1952**

Aims and Scope

ENGINEERING TRANSACTIONS promotes research and practise in engineering science and provides a forum for interdisciplinary publications combining mechanics with material science, electronics (mechanotronics), medical science and biotechnologies (biomechanics), environmental science, photonics, information technologies and other engineering applications. The Journal publishes original papers covering a broad area of research activities including experimental and hybrid techniques as well as analytical and numerical approaches. Engineering Transactions is a quarterly issued journal for researchers in academic and industrial communities.

Address of the Editorial Office:
Engineering Transactions
Institute of Fundamental Technological Research
Świętokrzyska 21,
PL 00-049 Warsaw, Poland

Phone: (48-22) 826 60 22, Fax: (48-22) 826 98 15, E-mail: publikac@ippt.gov.pl

Abstracted/indexed in:

Applied Mechanics Reviews, Current Mathematical Publications, Inspec, Mathematical Reviews, MathSci, Zentralblatt für Mathematik.

`http://et.ippt.gov.pl/`

SUBSCRIPTIONS

Address of the Editorial Office: Engineering Transactions
Institute of Fundamental Technological Research, Świętokrzyska 21
PL 00-049 Warsaw, Poland
Tel.: (48-22) 826 60 22, Fax: (48-22) 826 98 15, E-mail: publikac@ippt.gov.pl

Subscription orders for all journals edited by IFTR may be sent directly to the Editorial Office of the Institute of Fundamental Technological Research

Subscription rates

Annual subscription rate (2009) including postage is US $ 176.
Please transfer the subscription fee to our bank account: Payee: IPPT PAN,
Bank: PKO S.A. IV O/Warszawa,
Account no. 05124010531111000004426875.

All journals edited by IFTR are available also through:

- Foreign Trade Enterprise ARS POLONA ul. Obrońców 25, 03-933 Warszawa, Poland, Tel. (48-22) 509 86 38, 509 86 37
- RUCH S.A. ul. Jana Kazimierza 31/33, 01-248 Warszawa, Poland, Tel. (48-22) 532 89 00, Fax (48-22) 532 87 45
- International Publishing Service Sp. z.o.o ul. Noakowskiego 10 lok. 38 00-664 Warszawa, Poland, Tel./fax: (48-22) 625 16 53, 625 49 55

Warunki prenumeraty

Prenumeratę na wszystkie czasopisma wydawane przez IPPT PAN prowadzi Biblioteka. Bieżące numery można nabyć a także zaprenumerować roczne wydanie Engineering Transactions bezpośrednio w Bibliotece IPPT PAN, Świętokrzyska 21, 00-049 Warszawa, Tel.: (48-22) 826 60 22; Fax: (48-22) 826 98 15.

Cena rocznej prenumeraty z bonifikatą (na rok 2009) dla krajowego odbiorcy wynosi 176 PLN
Również można je nabyć, a także zamówić (przesyłka za zaliczeniem pocztowym) we Wzorcowni Ośrodka Rozpowszechniania Wydawnictw Naukowych PAN, 00-818 Warszawa, ul. Twarda 51/55, tel. (48-22) 697 88 35.

Wpłaty na prenumeratę przyjmują także jednostki kolportażowe RUCH S.A. Oddział Krajowej Dystrybucji Prasy, 01-248 Warszawa, ul. Jana Kazimierza 31/33, Konto: PBK S.A. XIII Oddział Warszawa nr 68124010531111000004430494. Dostawa odbywa się pocztą zwykłą w ramach opłaconej prenumeraty z wyjątkiem zlecenia dostawy pocztą lotniczą, której koszt w pełni pokrywa zleceniodawca. Tel.: (48-22) 620 10 39, fax: (48-22) 620 17 62.

Arkuszy wydawniczych 5.25; Arkuszy drukarskich 4.25
Papier offset. kl. III 70 g. B1
Oddano do druku w kwietniu 2009 r. Druk ukończono w kwietniu 2009 r.
Skład w systemie LaTeX K. Jezierska
Druk i oprawa: Drukarnia Braci Grodzickich, Piaseczno ul. Geodetów 47A
